TÉCNICO LISBOA

New approach to the preparation of zeolite-based catalysts for CO_2 methanation

Temiloluwa Ademuwagun

Thesis to obtain the Master of Science Degree in

Energy Engineering and Management

Supervisors: Dr. Ana Cristina Gomes Ferreira da Silva Parreira

Dr. Maria Del Carmen Bacariza Rey

Examination Committee

Chairperson: Prof. Francisco Manuel da Silva Lemos

Supervisor: Dr. Ana Cristina Gomes Ferreira da Silva Parreira

Member of the Committee: Dr. Carla Maria Duarte Nunes

October 2020

Special acknowledgement

This thesis is based on the work conducted within the Innoenergy Master School, in the MSc program Clean Fossil and Alternative Fuels Energy (now called Energy Transition). This program is supported financially by the Innoenergy. This author also received financial support from Innoenergy, which is gratefully acknowledged.

Innoenergy is a company supported by the European Institute of Innovation and Technology (EIT) and has the mission of delivering commercial products and services, new businesses, innovators and entrepreneurs in the field of sustainable energy through the integration of higher education, research, entrepreneurs and business companies. Shareholders in Innoenergy are leading industries, research centers, universities and business schools from across Europe.

www.innoenergy.com

MSc Clean Fossil and Alternative Fuels Energy is a collaboration of:

AGH University of Science and Technology, Krakow, Poland

SUT Silesian University of Technology, Katowice, Poland

IST Instituto Superior Técnico, Lisbon, Portugal

(The MSc thesis was prepared at Campi Alameda and Tecnológico e Nuclear of Instituto Superior Tecnico, Lisbon and Bobadela, Portugal)

Acknowledgements

I would like to thank my thesis supervisors, Dr. Ana Cristina Gomes Ferreira da Silva Parreira and Dr. Maria del Carmen Bacariza Rey; for their invaluable support, guidelines and encouragement, who in different ways, contributed to the successful completion of this thesis. Their impeccable supervision enabled the execution of this thesis. I say a big thank you from my heart.

Also, special thanks to my parents and siblings for their invaluable support and prayers throughout the whole process. To my amazing friends, Manuela, Abayomi, Olushola, Damilola and Deogratias, thank you for your encouragement and assistance in my work; without your support, finishing this thesis would have been no mean feat.

To all the friends I made throughout this program, thank you for being there and making studying abroad a bit more interesting.

Abstract

In today's scenario, biomethane, has increasingly grown popular worldwide as one of the foremost technologies for producing renewable energy from different biomass sources. Biomethane can be obtained from the purification of the biogas produced by the anaerobic fermentation of organic waste (30-60 wt.% CO_2 and 40-70 wt.% CH_4). Biogas upgrading is carried out by separating CO_2 from CH_4 through adsorption, absorption or even membrane processes. An alternative strategy is the valorization of biogas through CO_2 methanation reaction. For that suitable CO_2 methanation catalysts need to be developed, and in literature, zeolites constitute promising support materials.

This work studied the preparation of metal-based (Ni, Ru) zeolite (HUSY, CsUSY) catalysts by solvothermal method. Firstly, the optimization of metallic nickel nanoparticles obtained by this method was performed. The effects of PVP/Ni wt. ratio, reaction time and different precursor salts were investigated. Samples were characterized by X-ray diffraction, temperature programmed reduction (H_2-TPR) and nitrogen physisorption. CO_2 methanation performances were evaluated in a laboratory-scale unit under experimental conditions previous optimized.

The best conditions to obtained Ni^0 nanoparticles with sizes < 20 nm were using a PVP/Ni ratio = 5 and reaction time of 12 h. However, these conditions induced the destruction of the zeolite structure, which explained their catalytic performances, lower than those exhibited by equivalent catalysts prepared by impregnation method. Among all, CsUSY zeolite supported catalysts led to the best catalytic performance.

Keywords: Biogas upgrading, CO_2 methanation, Zeolite catalysts, Solvothermal method.

Resumo

Atualmente, o biometano tem-se tornado cada vez mais popular em todo o mundo como uma das tecnologias mais importantes para a produção de energia renovável a partir de diferentes fontes de biomassa. O biometano pode ser obtido a partir da purificação do biogás produzido na fermentação anaeróbia de resíduos orgânicos (30-60% de CO_2 e 40-70% de CH_4). A sua purificação (upgrading) é efetuada separando o CO_2 do CH_4 usando processos de adsorção, absorção ou membranas. Uma estratégia alternativa é a valorização do biogás através da metanação do CO_2. Para tal, catalisadores adequados necessitam ser desenvolvidos, e na literatura os zeólitos constituem suportes promissores.

Este trabalho estudou a preparação de catalisadores metálicos (Ni, Ru) suportados em zeólitos (HUSY, CsUSY) pelo método solvotérmico. Primeiramente, foi otimizada a síntese das nanopartículas de níquel através do mesmo método, onde foram estudados os seguintes parâmetros: razão PVP/ Ni (wt.), tempo de reação e diferentes sais precursores. As amostras foram caracterizadas por difração de raios-X, redução a temperatura programada (H_2-TPR) e fisissorção de azoto. O desempenho catalítico para a metanação de CO_2 foi avaliado numa unidade em escala laboratorial em condições experimentais otimizadas.

As melhores condições para obter nanopartículas de níquel com tamanhos <20 nm foram, usando uma razão PVP/Ni = 5 e um tempo de reação de 12 h. Estas condições levaram à destruição da estrutura do zeólito, o que pode explicar o seu inferior desempenho catalítico, comparativamente com catalisadores preparados por impregnação. Os melhores catalisadores foram os suportados no zeólito CsUSY.

Palavras-Chave: Purificação do biogás, Metanação do CO_2, Catalisadores suportados em Zeólitos, Método solvotérmico.

Index

List of Tables

List of Figures

List of Abbreviations

Al_2O_3 - Aluminum oxide

Bio-LNG- Bio-liquified natural gas

GHG- Greenhouse gases

IEA- International Energy Agency

IRENA- International Renewable Energy Agency

CH_4- Methane

CO_2- Carbon dioxide

CO- Carbon monoxide

He- Helium

H_2O- Water

H_2S- Hydrogen sulfide

NaOH- Sodium hydroxide

Ni- Nickel

Nm^3_{CH4}/t_{VS}- Norm cubic meter of methane per ton volatile

NP(s) – Nanoparticle(s)

OECD- Organization for Economic Co-operation and Development

O_2- Oxygen

PSA- Pressure swing adsorption

PV- Photovoltaics

PVP- Poly-(N-vinyl-pyrrolidone)

RE- Renewable energy

SiO_2- Silicon dioxide

SNG- Substitute natural gas

TSA- Temperature swing adsorption

TWh- Terawatt-hours

1. Introduction

1.1 Global Energy Sources Consumption

The world's energy demand has been increasing over the years, with fossil fuels being the major source of energy in the past years. Decades ago, the OECD countries made up for most of the consumption of energy in the world however, due to the increasing population, economic growth and increase in the standard of living in the Non-OECD countries, mostly India and countries in Africa in the coming years, energy consumption would still be on the rise [1]. Figure 1 shows the primary energy consumption presented from 1965 to 2018. In the beginning, the bulk of the consumption was by the OECD countries, North America, Eurasia and Europe [2]. Although their energy consumption is still increasing, their total share in the world's energy consumption has declined but has been steadily increasing for the rest of the world, especially in Asia Pacific whose consumption currently is approximately 45% of the total consumption.

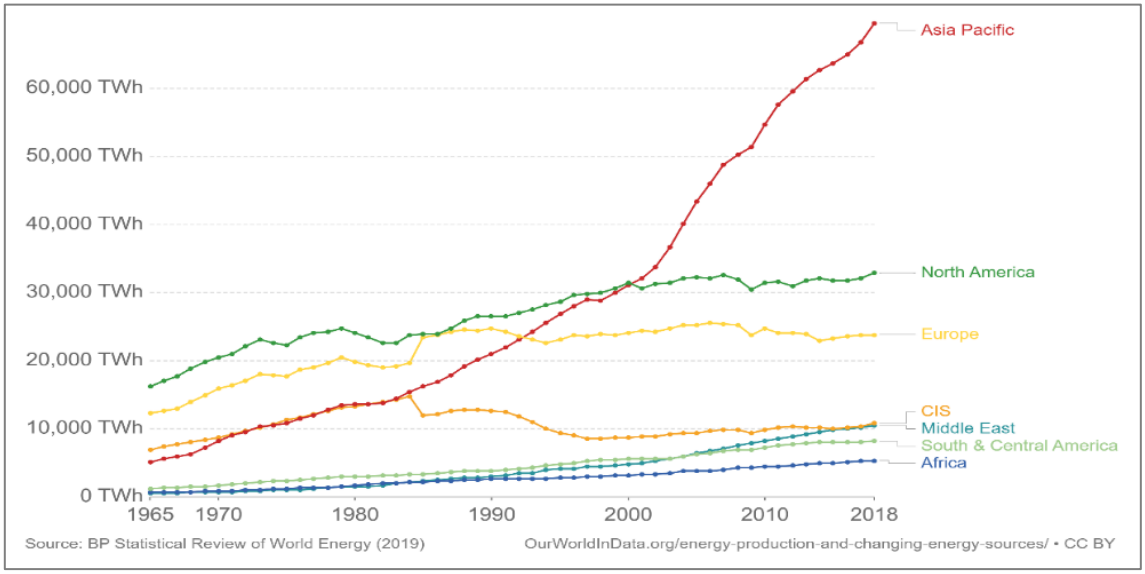

Figure 1: Primary energy consumption (terawatt-hours, TWh) by region from 1965 to 2018 [2]. Note that this data includes only commercially-traded fuels (coal, oil, gas), nuclear and modern renewable used in electricity production. As such, it does not include traditional biomass sources.

Majority of the world's energy supply comes from fossil fuels such as coal, oil and natural gas. As shown in Figure 2 below, traditional biomasses (e.g. wood and organic matter) were the only energy sources until other fossils fuels (e.g. coal, crude oil and natural gas) became the main suppliers of energy starting from the 1850s. Nuclear and renewable energy sources (e.g. solar, wind, biofuels and other renewables) joined the world's energy mix by the 1960s and 1970s, respectively. [2].

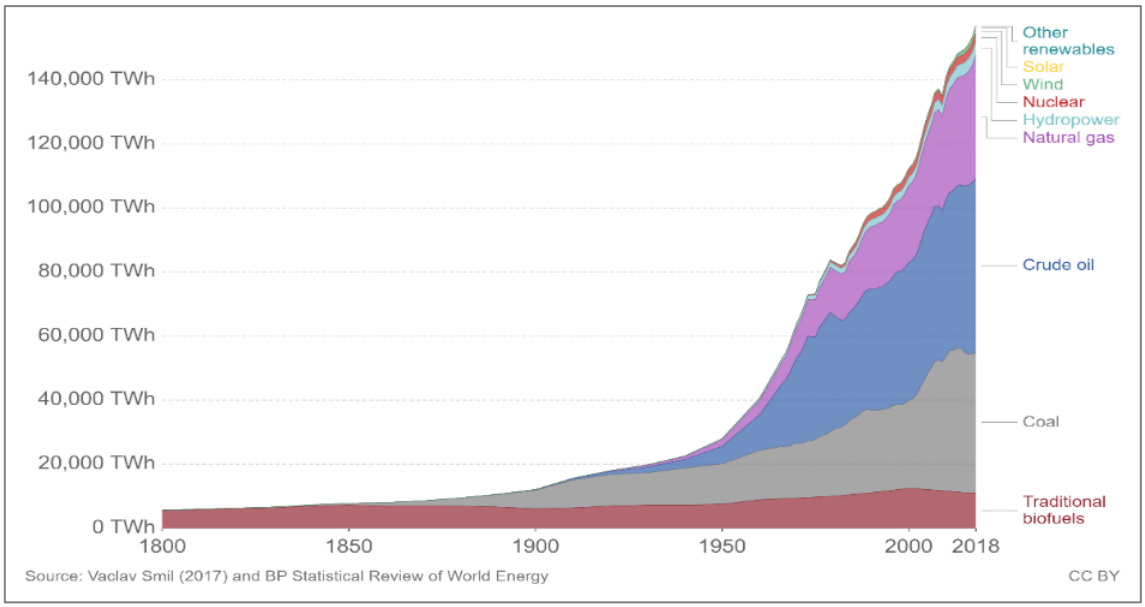

Figure 2: Global Primary Energy Consumption (TWh/year) [2]. Note that 'other renewables' refers to renewable technologies not including solar, wind, hydropower nor traditional biofuels.

In 2015, the energy consumed was about 25 times higher than the energy produced in the 1800s (140,000 TWh compared to 5600 TWh). From BP Statistical Reviews, in 2018, the global energy consumption grew at a rate of 2.9%, which is almost double its yearly average increase (~1.5%) since 2010/11, due to growth in the economy [3]. Also, carbon emissions from energy use grew at a high rate (2%, fastest growth for seven years) causing even more harmful effects to the environment [3]. This is due to the growth in energy demand from GDP (Gross Domestic Product) growth and increased industrial activity. In 2017, 80% of the growth in energy demand was because of Non-OECD countries and can be majorly attributed to China, its energy consumption almost tripled when compared with the past years.

1.1.1 Effect of Fossil Fuel on Climate Change

The discussion about climate change has repeatedly been in the news in the past years. About 65% of worldwide emissions of carbon dioxide (CO_2) and methane (CH_4) have been linked with 90 companies majorly dealing with carbon products which include 56 oil and gas producers, 37 coal extractors and 7 producers of cement [4]. However, due to the economic benefits of using fossil fuels, this has caused the pursuit for more reserves despite the obvious consequences on the climate.

Driven by higher energy demand in 2018, global energy-related CO_2 emissions rose by 1.7%, being the highest rate of growth since 2017 [5]. IEA (International energy Agency) analyzed the effect of fossil fuels use on global temperature increase and found that CO_2 emissions from coal combustion were responsible for over 0.3 °C of the 1 °C increase in global average annual surface temperatures above pre-industrial levels. In the electricity and heat sector, use of fossil fuels has resulted in 40% of the carbon emissions. [5]. They also contribute to the emission of sulphur oxides (SO_x), volatile organic compounds (VOCs), nitrogen oxides (NO_x), poly-aromatic hydrocarbons (PAHs) and particulate matter (PM-2 and PM-10), all of which contribute to global warming.

In most oil producing areas, it is more economical to burn off the natural gas into the atmosphere than to create management systems for its removal and storage. The total amount of gas flared just based on satellite data in 2011 was about 140 billion m^3 [6]. This is both wasteful and detrimental to the environment as methane still has damaging effects on the atmosphere and that amount of natural gas could be used to produce electricity. Apart from the effect on the climate, there is also the socio-economic effect to consider. Typically, when there is heavy reliance on one export commodity, such economies are known to be volatile and investment difficult, poorly distributed wealth and income is spent on ensuring there are buffers for shocks in the market.

The Paris Agreement states that the world should keep the global warming temperature below 2 °C and further to 1.5 °C [7]. Given the current emissions rate which is increasing rapidly, it is important to act as quick as possible otherwise the goal to keep global temperatures at below 2 °C may become unrealistic. As the search for better energy sources in order to mitigate carbon emission continues, the need to increase percentage of renewable energy sources in the overall energy mix cannot be over emphasized. Currently, renewable energy sources are being explored to meet the increasing demands of energy.

1.2 Renewable Energy Sources

1.2.1 Context

Energy use is responsible for about two-thirds of total annual GHG emissions. A closer look shows that power generation is responsible for the bulk of these emissions, followed by manufacturing and transport (see Appendix 1). A mitigation strategy which can be employed towards reducing emissions is the use of renewable energy sources for decarbonisation of the energy sector. Renewable energy sources (e.g. wind, solar, biomass) produce much lower emissions and will lead to improved public health [7], [8]. Some other benefits associated with renewables towards sustainable development include: energy security and access; social and economic development [9]. Furthermore, another advantage of renewables is higher productivity, which could translate into lower prices, stimulating more market growth for renewables and sustained demand for labour in the sector [7], [8].

Renewable energy (RE) has become a fundamental and growing part of the world's ongoing energy transformation. Increasingly, renewables have become the first choice for expanding, upgrading and modernizing power systems around the world. Using renewable energy is the prime choice to enhance access to affordable, reliable and cleaner source of energy. The maturity of the renewable energy market, technological development and policy refinement can provide the opportunity to develop a sustainable energy system. Illustrated below in Figure 3 [8] is the power capacity and growth rate of renewable energy from year 2000 to 2015.

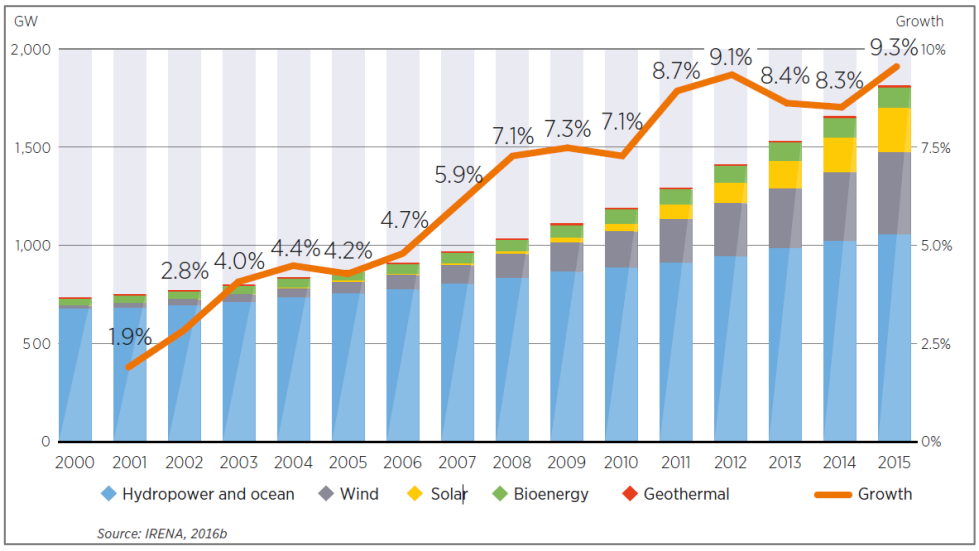

Figure 3: Renewable Power Capacity and Annual Growth Rate [8].

Renewables are energy sources that are continually replenished by nature and derived directly from the sun (e.g. thermal, photo-chemical), indirectly from the sun (e.g. wind, hydropower, biomass), or from other natural movements and mechanism of the environment (such as geothermal) [9], [10]. RE sources exclude the conventional energy sources such as fossil fuels or waste product from organic/inorganic sources. Different technologies are used to convert these natural energy sources into usable energy forms like electricity, heat and fuels. Figure 4 [10] shows an overview of the renewable energy sources. Nowadays, RE sources are vastly used for different purposes around the world such as electricity generation, to meet demand for heat and fuels for the diverse transport system [10].

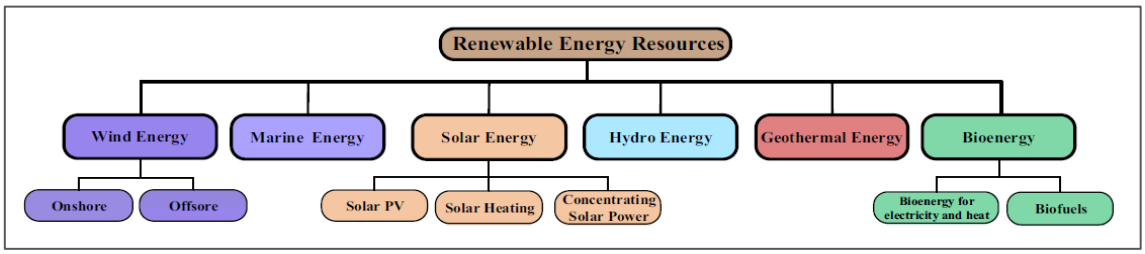

Figure 4: Overview of Renewable Energy Sources [10].

1.2.2 Types

- Wind Energy

The resource of wind energy potential is large but still uncertain [11]. Investment in wind power as an environmentally friendly and cheapest RE form is increasing globally [12]. Wind exists everywhere in the world, in some places with adequately high energy density. Basically, wind energy harnesses kinetic energy from moving air and with turbines, it converts the energy into useful forms such as electricity. To generate electricity from wind, the kinetic energy is firstly converted to mechanical and then electrical energy, it is quite challenging for industry to design cost effective wind turbines and power plants to

perform these operations. Based on recent studies, there are onshore and offshore wind energy technologies that are been investigated in order to improve the wind energy potential [9], [10].

- Solar Energy

Solar energy is collected from solar irradiance to generate electricity using photovoltaic (PV) and concentrating solar power, to produce thermal energy, in order to meet direct lighting needs and other purposes. The technological potential of solar energy applications is enormous, and a variety of systems are installed around the globe. In a PV system, there is a PV cell (semiconductor) that converts solar energy into direct-current electricity. PV systems are highly modular, i.e., modules can be connected to generate power up to tens of megawatts. Also, there are solar heating and cooling technologies that collect thermal energy from the sun and use this heat to provide boiling water, space heating and cooling for residential, commercial, and industrial applications [9]–[11].

- Hydropower Energy

Hydropower involves the movement of water from a higher to lower elevations, primarily to turn turbines and generate electricity in the process. Technologically, hydropower systems are proven to be well matured based on long historical experience with an estimated potential capacity of about 3721 GW/year, although the global installed capacity of hydropower is far less than its potential [9]. Hydropower projects, able to improve the socio-economic development of a country, are mostly site-specific and designed based on the river system they inhabit. Hydropower plants are classified into three categories in conjunction to the operation and type of water flow. Today, hydropower technology boasts with a high conversion efficiency and is extremely flexible [10], [11].

- Geothermal Energy

Geothermal energy, a reliable, cost-effective and environmentally friendly energy source [9], [10], is an efficient means of extracting RE naturally from the earth's interior as a heat source. The heat's origin relates to the internal structure of the planet and the physical processes occurring there. There is a large quantity of heat present in the earth's crust, not to mention the deepest parts, however, the heat is unevenly distributed and rarely concentrated. Tapping the energy can be done on a small scale using a geothermal heat pump, or on a large scale through a geothermal power plant.

- Biomass Energy (Bioenergy)

Biomass energy has a wide range of applications, being multiple research currently performed in this area [9]. Bioenergy can be defined as the conversion of biomass into usable energy forms like heat, electricity and liquid fuels (biofuels). Biomass for bioenergy comes either directly from land, such as from dedicated energy crops, or from residues generated fin the processing of crops for food or other products [10]. In addition, bioenergy is particularly unique because of its versatility and possibility to produce negative emissions when combined with carbon capture and storage systems [11]. Biomass refers to all organic materials derived from plants, trees and crops, and is essentially the collection and storage of the sun's energy through photosynthesis [10]. These materials can be broadly grouped into six major supply sectors: agricultural residue, dedicated energy crops, forestry, industry, parks and

gardens and waste [13]. Biomass has remained a vital energy source for mankind since the inception of civilization. Among the different renewable energy sources, biomass seems to have an edge over others as it competes most favorably in all countries of the world.

1.3 Biomass Valorization Routes

Presently, biomass represents about 10% of the global energy supply through RE sources, of which two-thirds are used in developing countries for cooking and heating [14]. Bioenergy is considered a sustainable energy source and has attracted much attention at global and national levels [15]. In plants, biomass is formed through conversion of CO_2 in the atmosphere into carbohydrates using solar energy. In the presence of light, green plants breakdown water to gain electrons and protons and then use them to convert CO_2 into glucose and oxygen is released as a waste product, this process is referred to as photosynthesis, Eq. 1 [16].

$$6CO_{2(g)} + 6H_2O_{(g)} \xrightarrow{SUNLIGHT} C_6H_{12}O_{6(s)} + 6O_{2(g)} \quad \text{Equation 1}$$

Biomass can be combusted directly to produce energy and can also be used as feedstock to produce a variety of liquid or gas fuels (biofuels). Biofuels such as biodiesel, bio-oil and biogas can be transported and stored, which helps to generate heat and power when required [10], [16]. This is of high significance, especially in an energy mix with relatively high dependence on intermittent energy sources (e.g. wind, solar). Also, biofuels contribute towards the goal of reducing dependence on fossil fuels as well as lowering the emissions of GHG [15].

The conversion route and any subsequent processing challenges that may arise are both determined by the biomass source's characteristics [15]. Also, the energy form produced depends on the type of biomass source. Since biomass can be utilized to meet a vast variety of energy needs including electricity generation, homes heating and fuels for vehicles, the processing technologies to convert it to biofuels is broadly divided into three categories, as shown in the Figure 5 [14], [15], [17].

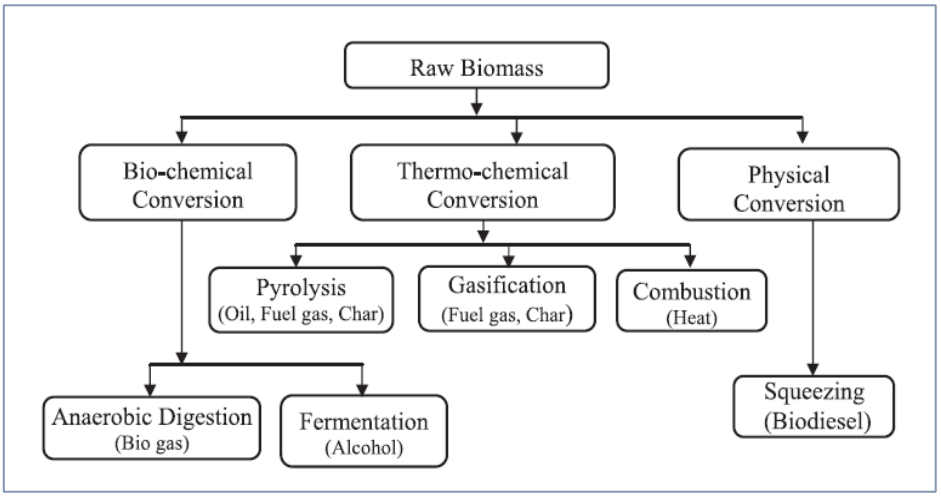

Figure 5: Biomass Conversion Routes [14].

Increasing the efficiency of biofuels production by using more advanced equipment is the necessary factor in extending biofuels utilization and doing further research by domestic institutes, private

companies and universities are actions to boost the production of biofuels and reducing the GHG emissions [12]. The processes for biomass conversion are briefly discussed below.

1.3.1 Thermochemical Conversion Process

Thermochemical conversion can be subdivided into three types: i) pyrolysis; ii) gasification; and iii) combustion. Pyrolysis is a process in which volatile components of a solid biomass are vaporized through heating without the presence of any oxidizing agent and a residue containing char and ash is left. After condensation, the condensate (pyrolysis vapor) is collected as a liquid which is known as bio-oil and the non-condensable gas remaining leaves the system and can be utilized as fuel gas. [14]. The major focus of the pyrolysis process is to acquire as much liquid product as possible from biomass. The liquid is then used for the production of chemicals, solvents and fuels. The product distribution of the bio-oil depends on the amount of cellulose, hemicellulose and lignin present in the biomass feedstock. Based on the operating conditions, pyrolysis can be grouped into three categories: fast pyrolysis, intermediate pyrolysis and slow pyrolysis [14], [18].

Gasification is the conversion of biomass through partial oxidation to produce fuel gas, which comprises carbon monoxide, hydrogen, carbon dioxide and methane as the main products. Possible gasifying agents include air, oxygen, steam or, in some cases, their combination [14], [17]. The major processes of biomass gasification can be divided into three stages: primary, secondary and tertiary cracking. In the primary cracking stage, syngas, carbon dioxide, methane and water would be produced as well as heavy tar rich in oxygenated vapors. Some gas products, light olefins and aromatics are generated from the secondary cracking. Thermal cracking of the heavy or light tar at high temperature would lead to the production of soot. [17].

Combustion is an exothermic reaction and produces heat and luminescence. Biomass is completely combusted alone in a dedicated plant, which is called direct combustion, or it can be co-combusted with coal in existing coal-based power plants that are co-firing to produce hot gases [14]. In combustion reaction, several processes like evaporation, mixture, diffusion and convection occur at a high velocity. Mostly, any biomass type can be combusted however, in practice, combustion is possible only for biomass having moisture level of less than 50%, unless the biomass is dried before. The main combustion product is heat, which can be used for power production [19].

1.3.2 Physical Conversion Process

In the physical conversion process, oil is drawn out mechanically by crushing the seeds of various biomass feeds. The process produces not only oil but also a solid residue called deoiled cake, which can be used for animal fodder. The extracted oil can be processed further by reacting it with alcohol to acquire biodiesel through a process called esterification [14]. The produced biodiesel could be a potential replacement for diesel from crude oil. There are several advantages of the biodiesel over the typical ones produced from petroleum such as higher flash point, faster degradability (up to four times) and no sulfur content.

1.3.3 Biochemical Conversion Process

This is the process by which biomass is converted to methane/carbon dioxide, fertilizer and water/ethanol using different microorganisms. Essentially, there are two biochemical processing ways for conversion of biomass into biofuel: i) fermentation; and ii) anaerobic digestion.

Fermentation is a metabolic process in which ethanol is produced from biomass conversion through enzymes. This process is used commercially for ethanol production from various types of feedstock that contain a favourable amount of sugar or any material that can be converted into sugar (e.g. starch or cellulose). Several studies have considered ethanol as the cleanest liquid fuel alternative to fossil fuels for transportation due to its oxygen content (~35%), which helps complete combustion of the fuel [20]. This reduces harmful emissions from vehicles. To convert lignocellulosic biomass into ethanol, there are four major steps to be taken, which are pre-treatment for the improvement of enzyme's accessibility, enzymatic hydrolysis for breaking down and conversion of the biomass to starch, fermentation with microorganisms such as yeast, and distillation to remove water content from the bioethanol produced.

As a biological process, the fermentation process depends on some factors, which include pH, temperature and oxygen, which affect the specific rate of growth [14], [19]. Conventional crops as corn, wheat and sugarcane can no longer meet the global demand for bioethanol due to population growth and industrial development. Thus, more research is being carried out on lignocellulosic biomass like forest and industrial residues, and agricultural waste, which could be used as feedstock for ethanol production by fermentation. Bioethanol production from rice straw, wheat straw, corn straw, and sugarcane has become a global interest with rice straw being the most abundant has the potential of producing a maximum amount of ethanol as compared to others [19].

Anaerobic digestion (AD) is a biological process of breaking down organic matter (in this case biomass) in the absence of oxygen to produce digestates and biogas, which consists mainly of methane and carbon dioxide with some traces of nitrogen and hydrogen sulphide, among all [19], [21]. The digestate obtained as a substrate from the production of biogas can be utilized as biofertilizer due to its composition (such as nitrogen, phosphorus, potassium). This type of sustainable energy production contributes directly towards the Sustainable Development Goals of the United Nations through waste recycling and energy delivery. The yield and composition of biogas is affected by the type of raw material used in the production process (Appendix 2).

Even though the AD process has been rapidly developing, there are still some problems that require solutions such as low biodegration efficiency, poor stability, long retention time and environmental stability [22], [23]. For the sake of clarity, Figure 6 [24] illustrates the life cycle of biogas. In the anaerobic process, the microorganisms decompose organic material through a series of metabolic reactions. First reaction is the hydrolysis of complex organics into soluble compounds. This is the limiting stage of the reactions process and, thus, a pretreatment of substrates is usually performed. Second reaction stage is known as acidogenesis. This is a breaking-down process of large organic polymers into organic acids (like sugar, amino acid, fatty acid) alcohols, hydrogen and carbon dioxide by acidogenic bacteria. [25]. Then, acetogenesis is the third reaction step where higher organic acids are broken down into acetic acid and hydrogen by acetogenic bacteria. Final reaction is methanogenesis, which involves the

production of methane by methanogenic bacteria. This reaction stage is the slowest as compared to others and it particularly important as the bacteria convert formic acid, acetic acid, methanol, carbon monoxide and carbon dioxide and hydrogen to methane [14], [19].

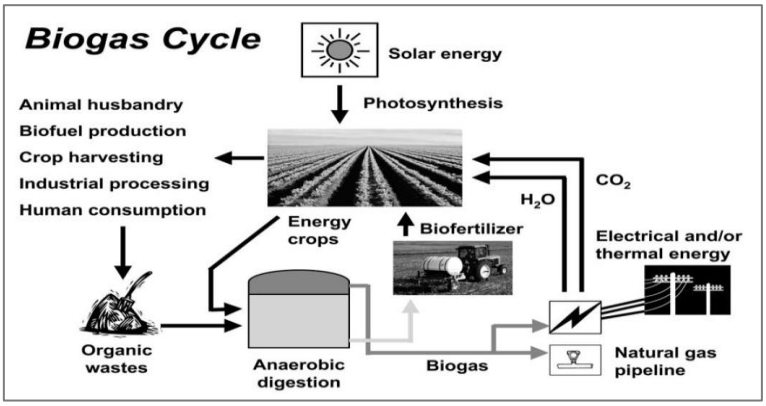

Figure 6: Biogas Cycle [24].

Anaerobic digester systems can be categorized into two main types, which are the single-stage reactor and the multiple-stage reactors. For a single-stage system, the important reactions happen in a single reactor simultaneously. On the contrary, in a multiple stage system the reactions occur sequentially in at least two reactors (see Appendix 3 for a typical schematic diagram of biogas digester). Some advantages of anaerobic digestion include feasibility to make use of biomass with high water content (up to 99%), and availability of conversion systems in smaller units [19]. The typical composition of raw biogas from anaerobic digestion is 45-70% of CH_4, 30-55% of CO_2, 0-5% of O_2, 0.01-6% of N_2, <3% of H_2O, 0-2000 ppm of H_2S and <100 ppm of NH_3. [25]. The high content of methane in biogas turns it into a suitable alternative to fossil fuels for electricity and heat generation, transportation fuel, and possible substitute for natural gas. Most research has been focused on improving biogas composition to increase the amount of methane composition, being this process called biogas upgrading [14], [26].

1.4 Biogas Upgrading (Biomethane As Natural Gas Substitute)

A promising way of using biogas is through its upgrading to natural gas, which is referred to as Substitute Natural Gas (SNG) or biomethane [27], [28], which has similar properties and uses to those of natural gas and can be injected directly into a natural gas distribution grid [27]. Presently, natural gas is the cleanest fossil fuel widely available and fitting to almost all end usage. Regrettably, it is not RE and generates carbon dioxide emissions. Biomethane, as it is obtained from biomass, is considered as a carbon neutral gas [29]. In addition, it currently counts towards the target of 20% renewable share of the final energy consumption from renewable sources by 2020 in the EU [30]. Biogas upgrading to biomethane involves the removal of CO_2 and all remaining trace compounds (e.g. H_2S, NH_3, N_2) in order to increase methane concentration, improving the energy density of the fuel.

1.4.1 Methods of Biogas Upgrading by CO_2 Removal

Biomethane produced by biogas upgrading needs to meet the gas quality specifications set by the European standard EN 16723-1 for injection into the gas grid or the quality specifications set in the standard EN 16723-2, to be used as Bio-LNG in road transport [30]. Various commercial technologies

can be utilized for removal of undesired elements and compound from biogas. The most popular technologies available at commercial scale are pressure swing adsorption (PSA), absorption (water scrubbing, physical sorption and chemical absorption), membrane separation and cryogenic separation [31]. The main focus of this section is summarizing the important details of technologies that involve the removal of CO_2 rather than giving explanatory details (for more details see Appendix 4). The choice of technology is based on the raw biogas composition, the size of the plant and cost of investment [27], [30], [32], [33]. Figure 7 [34] below shows the distribution of the various biogas upgrading technologies in Europe.

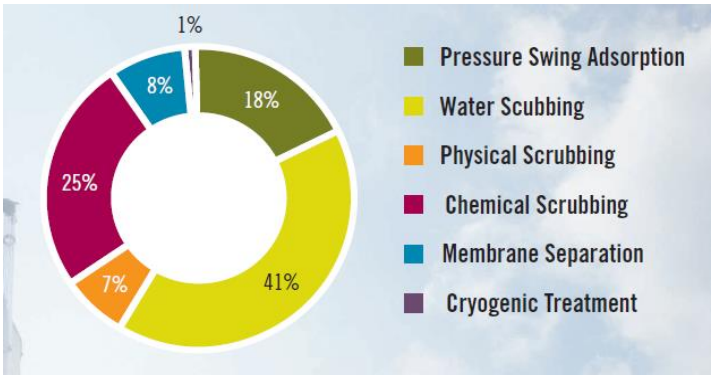

Figure 7: Distribution of Biogas Upgrading Technologies in Europe in 2016 [34].

The *Pressure Swing Adsorption (PSA)* technology is based on the selective adhesion of one or more constituents a gaseous mixture on the surface of a solid with micropores, typically equilibrium-base adsorbents [30]. Molecular sieve materials like zeolites and activated carbon are usually applied. The absorbent pores allow a free penetration of the CO_2 molecules, while filtering the larger CH_4 molecules on its surface. With this technique, a 95-99% concentration of methane is achievable [28], [30], [35].

Absorption technologies are based on the solubility of the gases contained in biogas, in a certain liquid. Water scrubbing is widely used to absorb CO_2 in physical absorption plants, whereas amine scrubbing is typically applied in chemical absorption [32]. Water scrubbing is used as an upgrading technique as well as pretreatment for the removal of hydrogen sulfide [30], [36]. Chemical scrubbing involves reversible reactions between absorbed substances and solvent. The most common solvent for biogas upgrading is amines: diethanolamine, mono-ethanolamine and methyl diethanolamine [37], [38].

Membranes are permeable barriers, specially designed to be the selective to certain molecules. This technique uses gas permeability to separate CH_4 from the other components of the gas [39]. The process propellers are concentration, pressure, temperature and electric charges of the different molecules. Basically, there are three types of membranes that are being used: polymeric, inorganic, and mixed matrix membranes. Inorganic membranes boast some advantages compared to polymeric, majorly because of their higher mechanical strength, chemical resistance and thermal stability [35]. *Cryogenic separation* is a technology used for gas separation and other large-scale industrial applications. The physical principle behind cryogenic separation is that gases like carbon dioxide and hydrogen sulfide liquefy under different pressure and temperature conditions. Cryogenic plants operate under a very low temperature (~170 ºC) and high pressure (~80 bar). [30]. Cryogenic process is still of interest for production road fuel, as it allows to produce Bio-LNG [40].

1.4.2 Biogas Upgrading with Direct CO_2 Methanation

In the previous section, the upgrading of biogas was based on the removal of CO_2, however, with technological advancement in the world today, perhaps there is a better alternative which can further explore the value of a raw biogas. As stipulated earlier (see section 1.4.1.3), a typical biogas composition ranges between 45-70% CH_4 and 30-55% CO_2 with some traces of a few other gases [41]. To exploit the large amount of CO_2 content in biogas, there is a proposed method for increasing the biomethane yield, which is by direct catalytic conversion of CO_2 into biomethane through methanation (Sabatier reaction, discovered by Sabatier and Senderens in 1902) using hydrogen produced from RE sources (e.g. solar radiation) through water electrolysis (Equation 2). This process of converting CO_2 to SNG contributes to the mitigation of global climate changes [42].

$$CO_{2\,(g)} + 4H_{2\,(g)} \leftrightarrow CH_{4\,(g)} + 2H_2O_{\,(g)} \qquad \Delta H_R = -165 kJ.mol^{-1} \text{ (at 298 K)} \qquad \text{Equation 2}$$

According to the literature, methane composition in the biogas has little influence on the reaction process when operated at moderate temperatures (below 400-450 ºC) where the reaction between CO_2 and CH_4 (dry reforming) is not favored [31]. It is also important to mention that the trace elements and compounds in the biogas should be removed first by prior gas treatment before methanation procedure takes place to avoid the deactivation of catalyst [43]. The typical catalysts used are metal-based materials (e.g. Ni, Co, Ru, Rh), supported on oxide matrices [43], see section 1.5.

In the last years, there have been several developments of carbon dioxide methanation reaction [41], [43], [44]. Indeed, CO_2 methanation is a widely known process within the energy industry and there are various pilot plants in operation, mainly in Europe. The operating temperature is usually around 250-450 ºC, while pressure ranges between 1-3 bar [45]. The methanation reaction is thermodynamically feasible, however, the reduction of carbon oxides to methane requires a catalyst to achieve acceptable rates and selectivity [41].

From literature studies [46], two mechanisms were mainly discussed regarding the methanation reaction. The first mechanism (dissociative) suggests that CO_2 dissociates to adsorbed oxygen and CO, and further to surface oxygen and carbon, which are then hydrogenated to produce methane and water. The second mechanism (associative) proposes that carbon dioxide is adsorbed over the catalyst's active sites in the form of carbonate species subsequently hydrogenated by H atoms provided by the active metal. This pathway proceeds typically through formate species as intermediates. These two mechanisms for CO_2 methanation are represented in Figure 8 [47].

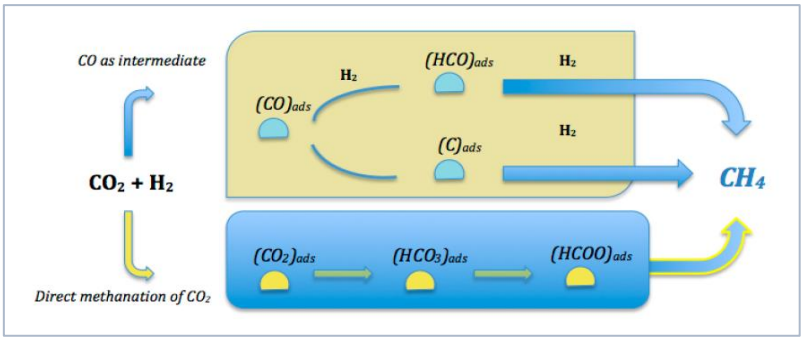

Figure 8: Mechanism of CO_2 Methanation Reaction [47].

The reaction route of CO_2 methanation is still under debate and some evidence shows that the nature of the metal, type of support, reaction intermediates and process conditions influence the reaction mechanism and its kinetics description [46], [48]. Kinetic studies performed over Ni and Ru based catalysts proposed diverse reaction mechanisms and steps (e.g. direct C–O bond and hydrogen assisted C–O bond dissociation) and thus a different rate of reaction expressions [46].

1.5 Catalysts for CO_2 methanation reaction

CO_2 methanation catalysts need to provide high activity at low temperature to avoid the formation of CO. As the process is quite exothermic, the catalyst must be resistant, especially against sintering which happens in the presence of high temperature and water, and deposition of carbon on the catalyst's active sites. Also, it is necessary that the catalyst is easy to synthesize for various industrial applications and easily recyclable [49].

Noble and transition metals such as ruthenium, rhodium, nickel and cobalt supported over different materials are the most studied catalysts for the CO_2 methanation reaction [48], [50]. Although ruthenium and rhodium have shown higher performances than nickel, most studies remain focused on improving the activity, selectivity and stability of Ni-based catalysts due to its lower cost and availability [46]. Table 1 summarizes representative CO_2 methanation catalysts developed in recent years [51].

Table 1: Summary of representative CO_2 methanation catalysts developed in recent years [51]–[54].

Catalysts	Preparation method [b]	Active metals content (wt.%)	Catalytic condition		Catalytic performance	
			GHSV (h^{-1})	*T/℃*	X_{CO_2}(%)	S_{CH_4}(%)
Ni/CeO_2	I	10	10 000	300	90	100
Ni/TiO_2	DP	15	2400	218	50	99
$Ni/\alpha\text{-}Al_2O_3$	I	20	9000	300	74	100
Ni/USY	I	14	43 000	400	66	94
Ni/ZSM-5	I	15	43 000	400	65	95
Ni/MSN[a]	I	5	50 000	300	64	100
Co/KIT-6	I	20	22 000	260	45	99
$Co0.4Ni/SiO_2$	I	10	13 200	300	58	-
$Ce_{0.95}Ru_{0.05}O_2$	Combustion	5	45 000	450	55	99
Ru-CeO_2/ Al_2O_3	I	2	10 000	300	60	99
Ru/TiO_2	BS	0.8	864	180	100	100
Ru/Al_2O_3	I	3	55 000	400	83	-
Ru/ZSM-5	I	2	-	350	100	100
$Ni\text{-}Ru/\gamma\text{-}Al_2O_3$	CP	Ni: 10; Ru: 1.0	9000	350	70	-

[a] MSN- mesostructured silica nanoparticles. [b] I- impregnation; CP- co-precipitation; BS- Barrel-sputtering; DP- deposition–precipitation. Pressure- 1 atm (0.1 MPa); GHSV – gas hourly space velocity.

As already pointed out, regarding the **active metals**, ruthenium is one of the most active catalysts for methanation process [47], [53], [55]. Its catalytic activity highly depends on the dispersion of the metallic phase (at high dispersion apparent activation energy becomes minimal), type of support and presence of promoters or modifiers, which can interact with the metal and even favor CO_2 adsorption/activation. Ru catalysts are highly selective towards CH_4 and, as seen in Table 1, the highest CO_2 conversion and selectivity to CH_4 at relatively low temperature was observed for the Ru/TiO_2 and Ru/ZSM-5 catalysts. Ru catalysts are known to be highly stable over a wide range of temperature and also very highly active towards methanation process, but fairly expensive [55], [56]. Furthermore, nickel catalysts are the most studied for CO_2 methanation because of their high efficiency, availability and low cost. According to [47], [53], [57], the effect of using different supports (α-Al_2O_3, MgO, TiO_2, and CeO_2) in the preparation of Ni catalysts has been studied. As stated in their reports, Ni/CeO_2 produced a high conversion of CO_2 at relatively low temperatures in comparison to Ni/α-Al_2O_3, and also had a selectivity to CH_4 of ~100%. Figure 9 shows the effect of supports on the yield of methane over Ni-based catalysts [53].

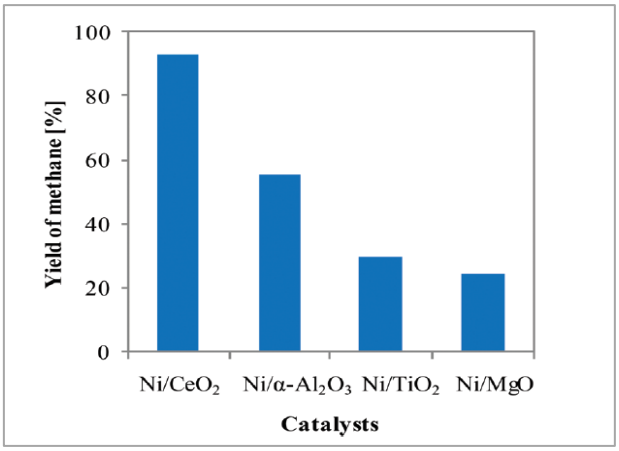

Figure 9: Effect of supports on yield of methane over Ni/CeO_2, Ni/α-Al_2O_3, Ni/TiO_2 and Ni/MgO tested under the same conditions: 350 ºC, 20 vol.% CO_2, 80% vol.% H_2 and GHSV=10 000 h^{-1} [53].

Catalytic activity needs the presence of Ni metal particles which may be formed *in situ* if the Ni loading is higher than the required to cover the surface of alumina with a complete monolayer according to the literature [53]. Authors suggested that, if Ni content is low, a pre-reduction treatment is needed. CH_4 selectivity of Ni catalysts with low Ni loadings was found to be high without CO formation [55]. Theoretically, the higher the Ni loading on a catalyst the greater the production of CO. However, it was found that small Ni^0 crystallites dispersed over alumina upon reduction achieved a high CO_2 conversion and selectivity to CH_4 was up to 100%. Further research has been carried out on nickel nanoparticles for CO_2 methanation process because nanoparticles sizes improved the dispersion of metal particles on support at low metal loading [55] which in turn enhances catalytic performance. Studies have reported that unsupported nickel nanoparticles performed poorly than supported ones [53], [55]. As mentioned by Sreedhar *et al.* [56], to increase the stability of Ni catalysts, promoters such as Pt, Pd and Rh could be added. These second metals prevented metal sintering and increased the dispersion of Ni particles, leading to higher CO_2 methanation yields [56].

According to Frontera *et al*. [47], metal nature plays an important role in the CO_2 methanation, both in activation and reduction steps [47]. Indeed, while active metals are typically responsible for H_2

dissociation, supports usually promote CO_2 activation and can induce a modification of the metal reducibility, electronic properties and dispersion, surface basicity or even hydrophobicity, which has allowed important enhancements of CO_2 conversion and CH_4 selectivity so far. Several parameters have been analyzed in order to optimize their properties of the catalysts such as using different supports, modifying the incorporation method and loading or even adding promoters [43], [47], [53].

The most commonly used types of **supports** in CO_2 methanation catalysts are Al_2O_3, MgO, ZrO_2, TiO_2, CeO_2 and SiO_2 [47], [55]. Also, combination of the already mentioned catalyst supports have been proposed [53]. Morphology of the active sites, adsorption ability and improving the catalytic features are the essential qualities of supports for effective methanation process [43]. High surface area materials such as silica, alumina, silica-alumina and zeolites have been extensively used in industrial processes for the preparation of metallic catalysts.

Zeolites, crystalline aluminosilicates with suitable chemical and textural properties for the methanation reaction, are among the possible supports that can be used in CO_2 methanation catalysts [53], [55]. Zeolite-supported catalysts have revealed promising results, especially due to their tunable properties in terms of basicity and hydrophobicity able to satisfy the characteristics necessary to achieve active, stable and selective materials for CO_2 methanation [58]. Also, this support enables the synthesis of catalysts with high surface areas (>300m^2/g) and pore volumes (around 1.7 and 300nm), favorable for this process [75]. Different zeolite structures could be used as supports and their basicity/acidity could be modified by ion-exchange with alkaline metals and by post-synthesis treatments [54].

The preparation of appropriate and well-defined zeolite catalysts, with controlled type of active sites (metals, metal oxides and acidity), could not only allow the utilization of zeolite's ability to stabilize different metal species, but also its confinement effects [54], [58]. These features of zeolite as a support make them suitable for diverse catalytic applications, however, a main drawback is that zeolite supports have been responsible for the formation of large Ni nanoparticles (25-30 nm), therefore further studies are required for improving the obtained metallic dispersion [54]. Taking into account that most zeolite-based catalysts for CO_2 methanation have been synthesized by the same method (impregnation), one possible strategy for achieving smaller metal particles is the study of alternative preparation strategies.

There are different methods of incorporating the active metals on supports, some of the most widely used being impregnation, sol-gel (single step or pseudo), ion-exchange, precipitation and combination of methods [55]. The sol-gel methods are mostly used in high temperature treatments for films and coating [59]. Additionally, solvothermal method allows the synthesis of Ni nanoparticles at low temperature without the protection of inactive gas, constituting a promising method.

1.6 Thesis objective

Amongst the different types of catalysts for CO_2 methanation, zeolite-based materials have revealed relatively high CH_4 yields during the reaction process. However, and considering that the main drawback of these catalysts, typically prepared by impregnation method, arises from the low metallic dispersion achieved so far in absence of promoters, the goal of this Master dissertation is to study a new approach

to the preparation of Ni and Ru supported on zeolite-catalysts for CO_2 methanation process by using the solvothermal method. To the best of our knowledge, this approach has not been tried before, representing a challenging and innovative strategy. The factors influencing the catalyst's synthesis will be investigated to determine optimal preparation routes. Catalytic testing will be carried out to evaluate their catalytic performance (CO_2 conversions and CH_4 selectivity).

2. Experimental Methodology and Materials

2.1 Preparation of metallic Ni nanoparticles and Ni/Zeolite catalysts

In this thesis, solvothermal method, a common procedure to synthesize inorganic nanoparticles (NPs) [59], was used for the preparation of metallic Ni NPs and Ni or Ru/Zeolite catalysts. For metallic Ni NPs synthesis [67], the feed components, including Ni precursor, ethylene glycol (used as reducing agent for the metallic ions), PVP ($[C_6H_9(NO)_n]$, molecular weight = 40 000, used as a nucleation-protective agent to avoid nanoparticles sintering and agglomeration) and NaOH pellets (used to adjust the pH value to ca. 12), [76], [77] were mixed together in predefined proportions (see Table 2). The obtained solution was then thoroughly mixed using a magnetic mixer until it became homogenous. The nickel salt (precursor) concentration was 0.05 M in the solution and, for the synthesis that included zeolites as support, the nominal composition of Ni was calculated to obtain 15 wt.%. The ratio of PVP to nickel used in the synthesis processes can be found in Table 2.

Afterwards, the solution was placed in an autoclave and heated at 180 °C (with an increase of 10° per minute) to reduce the Ni ions and form to Ni atom (metal). Consequently, the product obtained was allowed to cool down to room temperature. There was an observation in the change of color for the solution, which indicates nucleation and growth. The obtained product was then centrifuged with excess ethanol at 2750 rpm for 5 min in a centrifuge. This process was repeated for approximately 3-5 times for the liquid to be properly separated from precipitate. Once the centrifugation process was completed, the product was further dried in a vacuum system installation at 70 °C using liquid nitrogen.

2.1.1 Optimization of Ni nanoparticles preparation conditions

As a first step, and in order to study the Ni precursor salts effect on the size of the metallic nickel nanoparticles, three different salts were used: nickel(II) chloride hexahydrate [$NiCl_2 \cdot 6H_2O$], nickel(II) nitrate hexahydrate [$Ni(NO_3)_2 \cdot 6H_2O$] and nickel(II) acetate tetrahydrate [$Ni(Ac)_2 \cdot 4H_2O$], each with purity above 98%. Properties of the reactants, such as their solubility and reactivity, change in the organic solvent or water at elevated temperatures and pressures. Reaction parameters such as pH, reaction time (t) in the autoclave, and PVP/Ni ratio (wt. ratio) were tuned to attain satisfactory particle size distribution. The prepared Ni NPs and the conditions used are presented in Table 2.

Table 2: Test conditions for preparation of metallic Ni nanoparticles.

Nickel precursors	PVP/Ni precursors ratio	Reaction time, h
$NiCl_2 \cdot 6H_2O$	0, 2, 4, 5	12, 20, 24
$Ni(NO_3)_2 \cdot 6H_2O$	5	12, 20
$Ni(Ac)_2 \cdot 4H_2O$	5	12, 20

2.1.2 Ni-zeolite catalysts preparation

In this work a USY zeolite provided by Zeolyst with a Si/Al ratio of 38 (CBV 780) has been used as support both in commercial (HUSY) and Cs-exchanged (CsUSY) forms, previous prepared. Bacariza *et*

al. mentioned that high Si/Al ratio favors catalytic performance as hydrophobicity property of the zeolite tend to increase, whereas zeolites basicity was considerably higher for lower Si/Al ratios [54]. The HUSY was prepared by ion-exchanging a certain mass of the zeolite with a NH_4NO_3 solution, keeping it under stirring and reflux during 4 h at 100 ºC. After that, the sample was filtered, washed with distilled water until pH = 7, dried overnight at 100 ºC and calcined. The CsUSY was prepared out by following an equivalent procedure to the one previously described, using the correspondent nitrate precursor salt [54], [70]. Their main textural properties can be found in Table 3. For the preparation of Ni/zeolite catalysts, the Ni precursor selected was nickel chloride, Table 4 presents the experimental conditions evaluated. For the preparation of Ru/zeolite catalysts, the Ru precursor chosen was ruthenium chloride. The preparation conditions are similar to that of Ni in Table 4 however only at reaction time of 12 h. Furthermore, the nominal composition of Ru was calculated to obtain 3 wt.%. Samples were named as $M/CCUSY_t$, where M refers to the active metal (Ni or Ru), CC corresponds to the compensating cation (H^+ or Cs^+) and t is the reaction time (12 or 20 h). For example, $Ni/CsUSY_{12h}$ corresponds to a catalyst with 15 wt% Ni, supported over CsUSY zeolite and prepared using a reaction temperature of 12 h.

Table 3: Main textural properties of the USY zeolite used in the present study.

Label	V_{micro} (cm^3/g)	V_{meso} (cm^3/g)	S_{BET} (m^2/g)
HUSY	0.208	0.271	450
CsUSY	0.194	0.295	579

Table 4: Preparation conditions of supported catalysts.

Zeolite	PVP/Ni precursors ratio	Reaction time, h
HUSY	5	12, 20
CsUSY	5	

For the purpose of further evaluation, mechanical mixtures of CsUSY zeolite and Ni NPs synthesized using 12 and 20 h of reaction time were prepared. The Ni NPs and support were mixed to achieved 15 wt.% Ni over CsUSY.

Also, for comparison purposes, the catalytic performances obtained for three reference catalysts, containing 15 wt.% Ni over HUSY and CsUSY and 3 wt.% Ru over CsUSY, previously prepared by incipient wet impregnation method will be presented. Samples were named as $Ni/CsUSY_{Imp}$, $Ni/HUSY_{Imp}$ and $Ru/CsUSY_{Imp}$.

2.2 Catalysts Characterization

2.2.1 X-Ray Diffraction (XRD)

X-Ray diffraction (XRD) is a technique commonly applied for the identification of phases in a material [60]. About 95% of all solid materials can be described as crystalline. Through an XRD experimental procedure, one can learn if one sample is (at least partially) crystalline and how many and which crystalline phases are present [61]. When a crystalline solid is submitted to X-ray, layers of periodically spaced atoms act as a diffraction grating. Thus, a physical scattering process happens when an

incoming wave excites the electrons of an atom that emits radiation of the same wavelength but in a different direction from that of the incoming wave. A diffraction peak appears when the path difference of the two rays scattered at the first and second layers of atoms is an integral multiple n of λ (wavelength). In this case, the interference will be constructive, and the diffraction peak will be produced for an incident angle θ as shown in Figure 10.

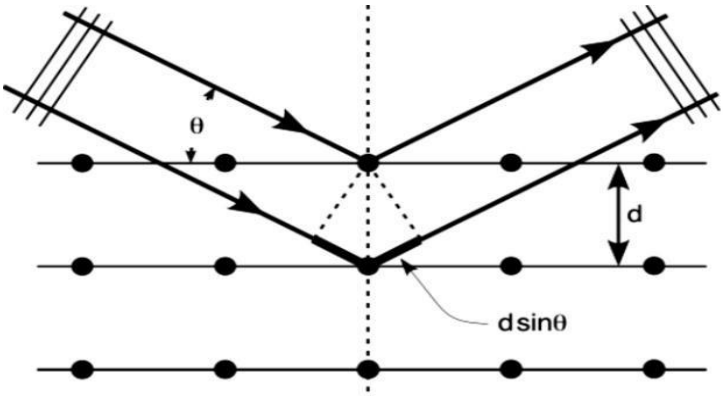

Figure 10: Geometric derivation of the Bragg equation for two layers of atoms with an interlayer spacing d.

Regarding Ni metal and zeolites, their unique structure in terms of atom positions and unit cell dimensions are reflected in the characteristic positions and relative intensities of the peaks observed, which can be found in the appropriate database for comparison purposes. As a result, the structure of a particular Ni metal and zeolite samples can be identified by comparing the experimentally measured powder diffractograms with reference patterns [62]. Furthermore, the integration of the intensity in a 2θ range where the characteristic diffraction peaks of a substance appear can be used to determine the crystallinity of the sample. Additionally, the full width at half maximum of diffraction peaks (FWHM, rad) can be used to estimate the average crystallite size of the metallic Ni nanoparticles and supported catalysts using Scherrer's equation [62].

Finally, regarding the experimental apparatus, the basic components of a diffractometer are an X-ray source, a monochromator, a goniometer for varying the angle, a sample holder system and a detector. Typically, X-ray tubes, in which electrons are emitted form a tungsten filament and accelerated by high voltage towards a water-cooled metal target, are used for the generation of X-ray. The energy of the incoming electrons is absorbed by exciting core electrons of the metal atoms. The generated core holes are refilled with electrons from outer shells, leading to characteristic X-ray emission lines. The most widely used target material is copper metal and the overwhelming number of XRD patterns are recorded using Cu K_α radiation of λ = 1.5418 Å for the K_α doublet, which is selectively reflected by a monochromator crystal positioned at a fixed Bragg angle. Furthermore, the sample is placed in the middle of the goniometer circle and the incident angle of the X-rays is varied. This can be achieved by arranging the components in different geometries. The classic geometry for powders and pellets is the one where a divergent primary beam illuminates a relatively large sample area, which decreases with increasing diffraction angles (unless variable slits are used) [61].

In the present work, powder X-ray diffraction was applied in order to get information about the type of phases present on the prepared Ni metal and catalysts, as well as to the identification of any damage

on the zeolites structure and the determination of average Ni sizes. The powder XRD patterns of nanoparticles (Ni or Ru) were obtained in a Bruker D2 Phaser diffractometer with a copper radiation source (Cu Kα, λ = 1.5406 Å) and operating at 30 kV and 10 mA. The scanning range was set from 20 to 80 ° (2θ), with a step size of 0.02 º and a step time of 0.8 s. Phase identification was carried out using the reference database software. For zeolite catalysts, the powder XRD patterns were obtained using a Bruker AXS Advance D8 diffractometer equipped with a 1D detector (SSD 160) and using a Ni filter. The scanning range was set from 5 to 80 ° (2θ), with a step size of 0.03 º and a step time of 0.5 s.

2.2.2 Temperature Programmed Reduction under H_2 (H_2-TPR)

The H_2-TPR allows the investigation of the catalysts reducing properties. It is a destructive method and often characterizes not only the surface but also, at least partially, the bulk. A quantitative setup (flow system and reproducible collection of the gases) will provide data for the calculation of the reducing properties, the dispersion, and the average oxidation state of the active particles [61]. When H_2-TPR experiments are carried out for metal-based catalysts supported on zeolites, useful information about the reducibility of the metal species present on the catalyst can be obtained. In this technique, H_2 is circulated through a catalysts bed while a temperature program is running, and its consumption is continuously analysed.

In principle, during a H_2-TPR experiment, a reducing mixture containing H_2 flows through a fixed amount of catalyst (where the active metal is present as an oxide or other reducible form) contained in a reactor which is linearly heated. The amount of hydrogen consumed during the reaction is given by the difference of its concentration in the mixture before and after reduction and is measured by a thermal conductivity detector (TCD). In order to obtain quantitative data, the gas mixture leaving the reactor passes through a cold trap before going to the TCD detector, to remove H_2O or other reduction products and a proper calibration has to be performed, for instance by injecting known amounts of H_2 through a sampling valve. The changes in the hydrogen concentration and the temperature with time are recorded being obtained the H_2-TPR profile. These H_2-TPR profiles are usually characterised by the occurrence of one or more reduction peaks that reflect the ability of the metal species to be reduced, the location of the different species in the support and also the kind of species present in the catalyst [63].

Additionally, H_2-TPR experiments provide very useful information to decide the proper reduction conditions of the metal oxide precursor and to recognize the presence of different precursor phases, their oxidation state and their interaction with the support. Therefore, H_2-TPR patterns can be used to study and optimize catalyst pre-treatment. In industrial laboratories, H_2-TPR is used as a quality control device to determine the efficacy of the preparation procedures [63]. In this work, H_2-TPR measurements were carried out in a Micromeritics AutoChem II using around 0.150 g of catalyst in every experiment. Catalysts were pre-treated under argon flow (25 ml min^{-1}) at 250 ºC (step 1), with a ramp of 10 °C/min and then cooled down to the room temperature (step 2). Then, H_2-TPR (step 3) was carried out by flowing 30 ml min^{-1} of a 5%H_2/Ar flow and raising the temperature from room temperature to 900 °C, at 10 °C/min (see Figure 11 [64]).

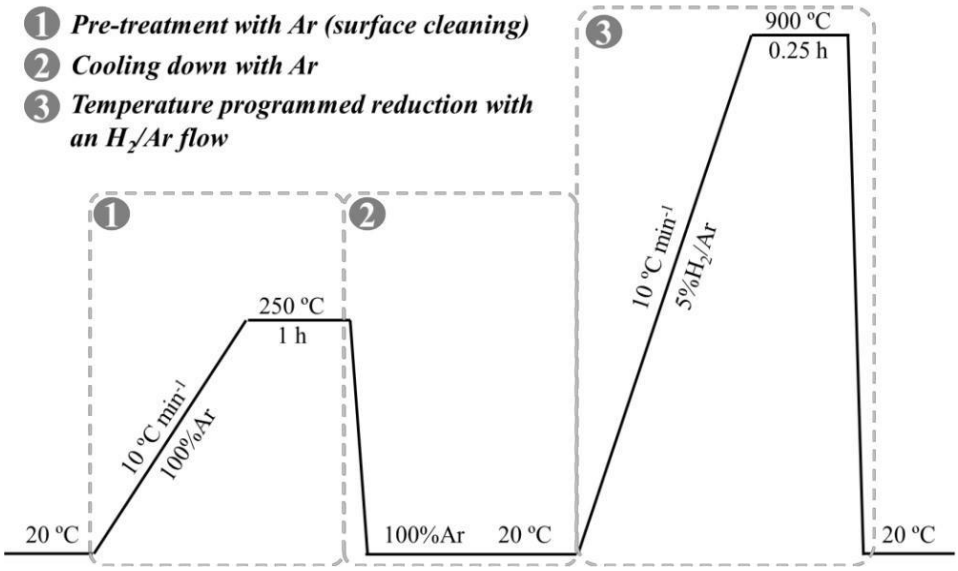

Figure 11: Scheme of the H_2-TPR procedure.

2.2.3 N_2 Physisorption

The specific surface areas of catalysts samples with support were determined by the Brunauer-Emmett-Teller method (the equation is described below [65]) and the measurements were carried out using a Micrometrics ChemiSorb 2720 – ChemiSoft TPx system. The samples were subjected to a flux of 30%N_2/He (P/P_0=0.3) at 20mL/min.

$$S_{BET} = \frac{S_t}{a} = \frac{v_m \times N \times s}{V}$$ Equation 3

where: S_{BET}- specific surface area; S_t- total surface area of sample material; a- mass of sample; v_m- monolayer absorbed gas volume; N- Avogadro's number; s- cross-sectional area of adsorbed gas molecule; V- molar volume of adsorbed gas.

The carrier gas was circulated through a fixed amount of catalyst contained in a reactor. For each catalyst, three tests (~ 0.100g of catalyst) were carried out and three cycles of N_2 adsorption (negative) and desorption (positive) recorded. The process involves the adsorption of N_2 and the formation of a monolayer at the temperature of liquid nitrogen, followed by desorption of N_2 after removing the liquid nitrogen and heating the sample to room temperature. The surface area was calculated based on the desorption peaks using the Micromeritics software installed, through a calibration curve (y=0.4367x+0.0004) previously prepared using the addition of known N_2 volume and recording of the detector's response, which allows, from the areas measured for the desorption peaks (x), to calculate the volume of N_2 adsorbed (y).

2.3 Catalytic Testing

2.3.1 Experimental Unit

The scheme for the catalytic setup used in the evaluation of catalytic performances is shown in Figure 12 [64]. Samples were placed in a pyrex reactor, where a thermocouple was inserted close to the

catalyst bed and positioned inside a TermoLab electric oven connected to a temperature program controller. All Gases (N_2, H_2 and CO_2) were supplied by Air Liquid with purities above 99.999% and regulated using mass flow controllers supplied by Brooks.

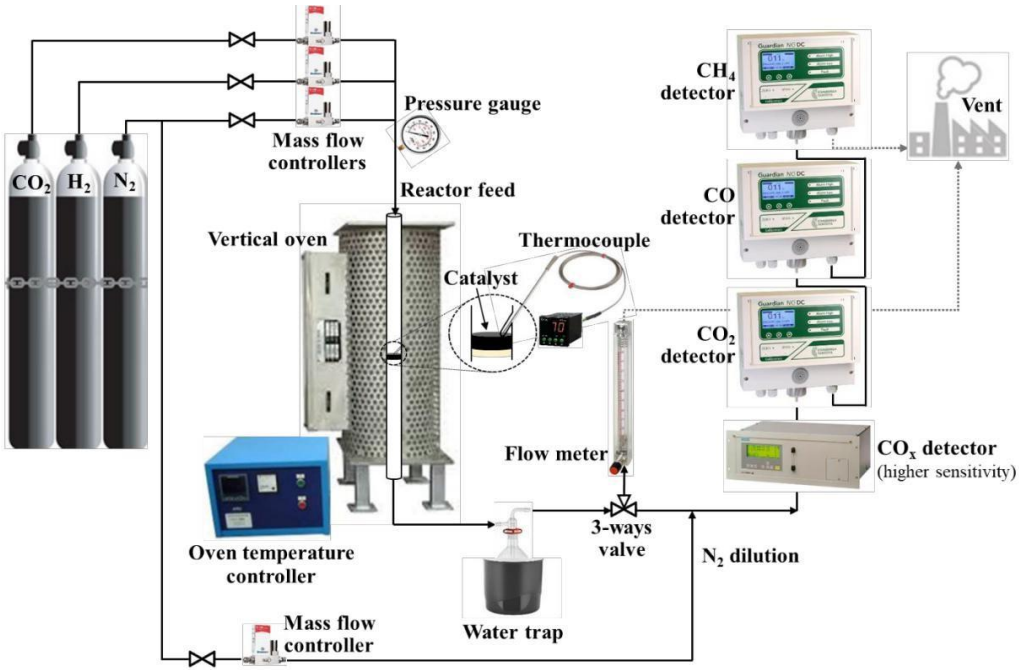

Figure 12: Scheme of the catalytic test unit.

2.3.2 Operating Conditions

Catalytic tests were performed using a fixed mass of catalyst (0.200 g) at atmospheric pressure. The temperature profile regarding the tests can be found in Figure 13 [64]. As seen, in-situ pre-reduction was generally performed at 470 ºC for 1 h (heating rate of 5 ºC min^{-1}) with 80%H_2/20%N_2 flow of 250 ml min^{-1} to get metallic Ni^0 species (step 1). In the case of the mechanical mixtures (MM) of zeolites and nickel nanoparticles no pre-reduction step was carried out. CO_2 methanation (step 2) was carried out between 250 and 450 ºC, keeping a reaction feed gas of H_2, CO_2 and N_2 at a molar ratio of 36:9:10 (stoichiometric ratio between H_2 and CO_2, total flow = 290 ml min^{-1}). The total flow over catalyst mass corresponded to 87000 ml h^{-1} g^{-1}. For each reaction temperature, after stabilization of catalytic system average value of the required data was taken for calculation of CO_2 conversion and CH_4 methane selectivity.

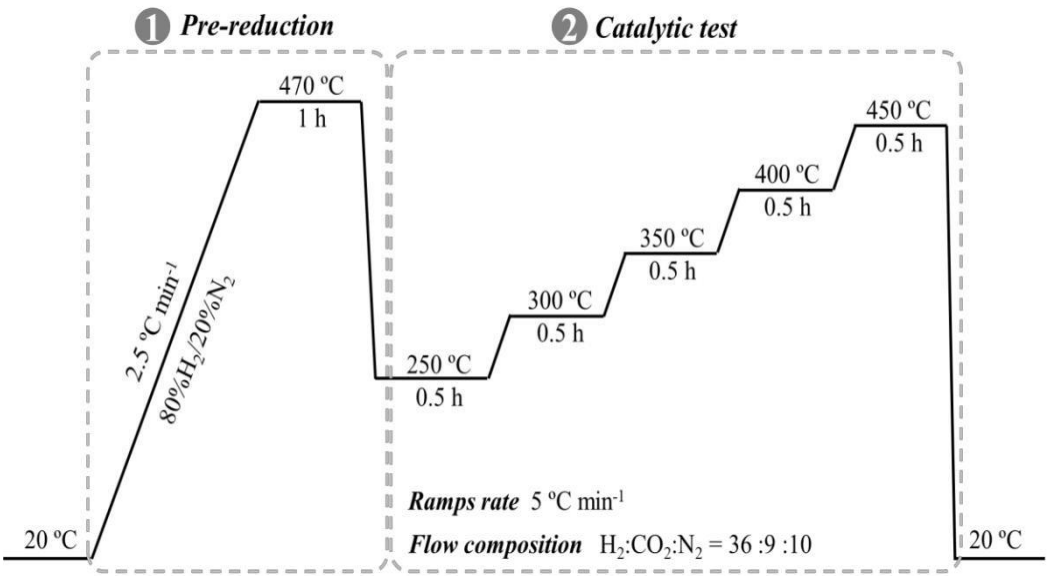

Figure 13: Temperature program of the catalytic tests accomplished in the present work.

2.3.3 Determination of the CO_2 Conversion and CH_4 Selectivity

Conversion of CO_2 (reactant) is calculated as the ratio of the moles of CO_2 converted per unit time to the molar flow rate of CO_2 fed and multiplied by 100. The equation for the conversion can be defined as:

$$CO_2\ conversion\ (\%) = \frac{F_{CO_2,inlet} - F_{CO_2,outlet}}{F_{CO_2,inlet}} \times 100 \qquad \text{Equation 4}$$

Furthermore, selectivity of CH_4 as the desired product is defined as percentage (%) of CO_2 which reacted to give CH_4. The selectivity to CH_4 (and CO) were calculated as shown below:

$$CH_4\ selectivity\ (\%) = \frac{F_{CH_4,outlet}}{F_{CO_2,inlet} - F_{CO_2,outlet}} \times 100 \qquad \text{Equation 5}$$

$$CO\ selectivity\ (\%) = \frac{F_{CO,outlet}}{F_{CO_2,inlet} - F_{CO_2,outlet}} \times 100 \qquad \text{Equation 6}$$

The detailed calculate ion of the conversion and selectivity for a certain $T_{reaction}$ can be found in Appendix 5.

3. Results and Discussion

To summarize, the scheme of the preparation procedures followed for the studies carried out in this work is illustrated in Figure 14. Firstly, in this chapter the main results presented correspond to the optimization of nickel nanoparticles (NPs) synthesis conditions, that will properly be discussed. Then, after determining the most promising preparation conditions, the characterization and catalytic performances exhibited by the Ni/zeolite catalysts will be presented. Finally, the effect of the metal nature (Ni or Ru) will be analyzed.

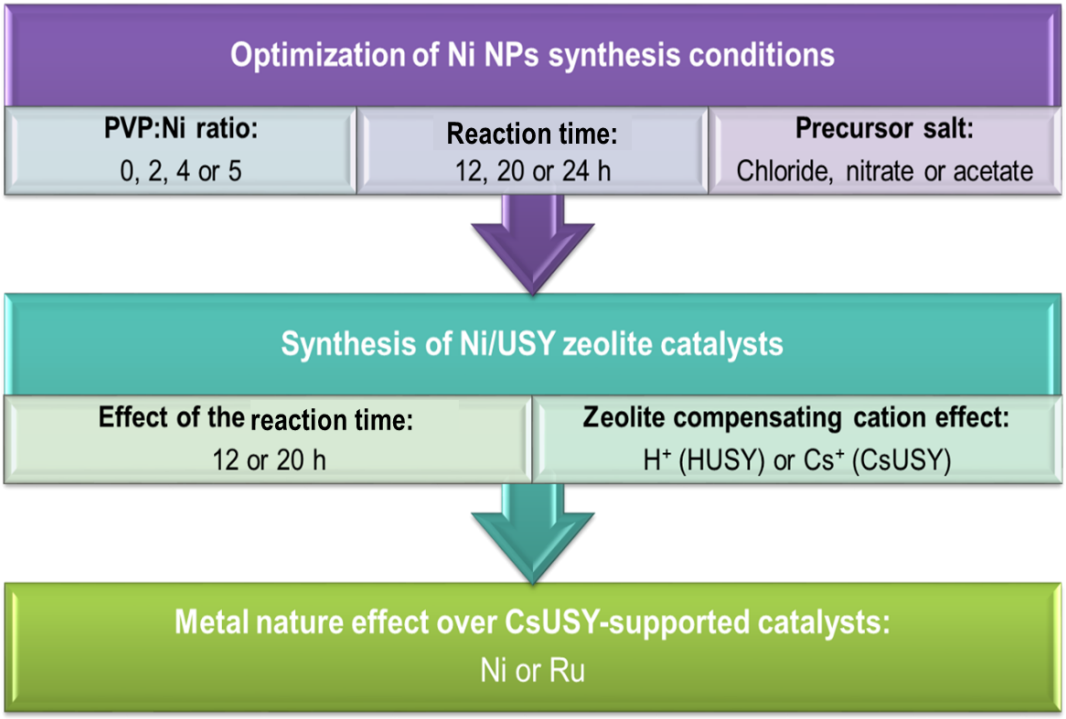

Figure 14: Summary of the studies accomplished in this work.

3.1 Optimization of Ni NPs synthesis conditions

To determine the optimal preparation route to produce the Ni/zeolite catalysts, metallic Ni NPs were firstly prepared with varying the PVP/Ni precursor ratio, the reaction time and Ni precursor salts, as described in previous section 2.1.1 (see Table 2). Ferromagnetic behavior was observed in the synthesized Ni NPs. The obtained metallic Ni NPs were then characterized by XRD to analyze the effect of different factors on the NPs composition and estimate the NP sizes.

Effect of PVP/Ni ratio

Figure 15 shows the XRD patterns of the synthesized Ni NPs with varying PVP/Ni ratios (0, 2, 4 and 5) and reaction time of 20 h. This is possible to observe three diffraction peaks with 2θ values of 44.5°, 52.1° and 76.5°, which correspond to the Joint Committee on Power Diffraction Standards (JCPDS) card no. 04-850 for metallic nickel [67]. Unfortunately, sample 0PVP/Ni_{20h} showed an additional diffraction peak with 2θ values of 47.2° which corresponds to silicon (Si) (JCPDS no. 27-1402) [66]. The

detection of Si in the XRD pattern can be explained as a result of the sample holder's problem during the XRD analysis.

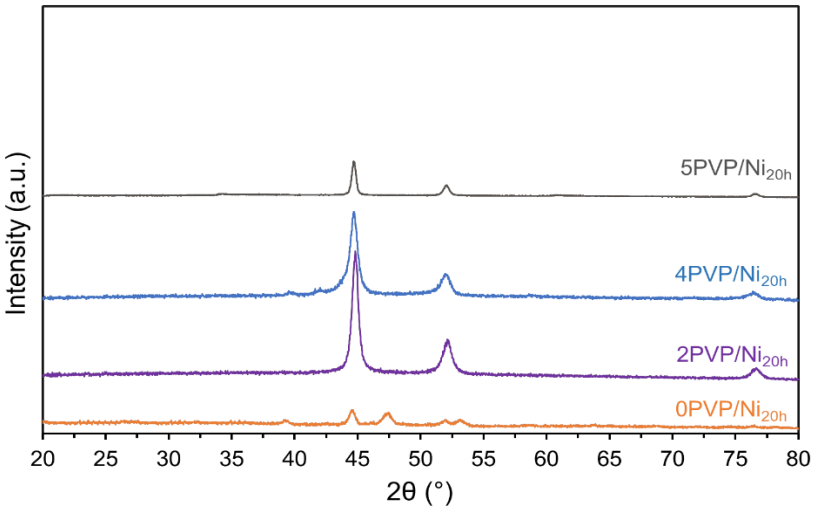

Figure 15: XRD patterns for 20 h reaction time Ni NP samples.

Furthermore, XRD analysis data was used to estimate the average nickel nanoparticle sizes by applying Scherrer's law (using the maximum intensity peak that corresponds to 2θ values of 44.5°, *hkl* 111). The results obtained are presented in Table 5. As expected [67], it can be observed that there is a decrease in particle sizes as the PVP/Ni ratio increases up to 4. At PVP/Ni=5, an increase in the particle size is noted. This can be attributed to the possibility of sintering of the NPs sample in the autoclave causing the particle size to increase. Also, the increase may be due to the washing process of the precipitate, which might not have been enough to remove all PVP. The influence of reaction time on the particle sizes was further investigated.

Table 5: Particle sizes of Ni NPs synthesized at 20 h reaction time.

PVP/Ni	Particle size (nm)
0	19.0
2	17.5
4	14.9
5	17.5

Effect of reaction time

The XRD patterns obtained for the Ni NPs prepared with the aim of optimizing the reaction time are presented in Figure 16. Results confirm the presence of mainly metallic nickel phase with no additional diffraction peaks. Based on this data and as previously done, average particle sizes were determined (Figure 17). As observed, at higher reaction times the particle sizes were similar, with no tangible difference between them. This result led to the conclusion that reaction times do not lead to a significant impact on the NPs size. Nevertheless, it is necessary to select an appropriate reaction time that allows complete growth and nucleation of the reactants to achieve total reduction.

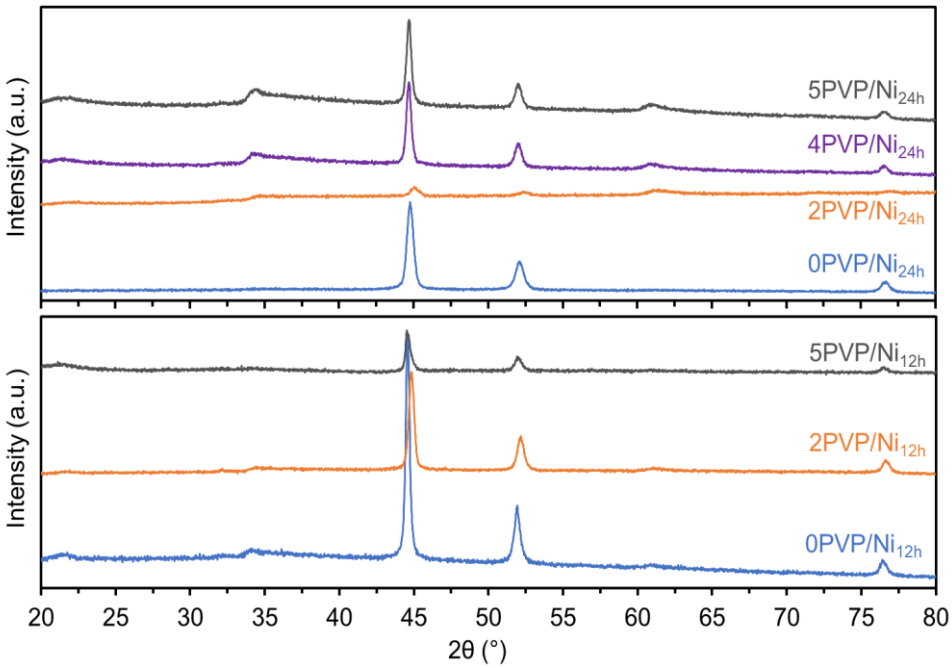

Figure 16: XRD patterns for Ni NP samples at 12 and 24 h reaction time.

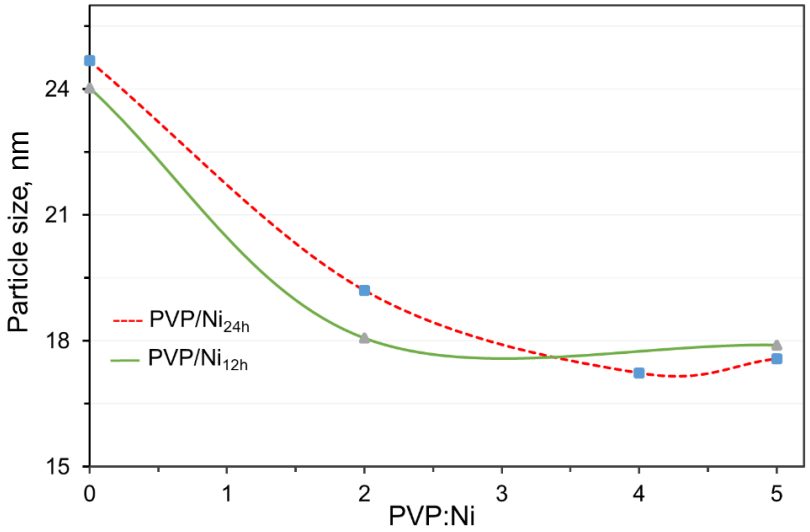

Figure 17: Nickel NPs sizes against PVP/Ni precursor ratio with reaction times of 12 and 24 h.

Effect of Nickel salt

According to Bayrakdar *et al.* [67], catalysts prepared by the solvothermal method are significantly affected by the choice of their metal precursor. Therefore, different Ni precursors were used to synthesize the Ni NPs to study and analyze how they affect the particle sizes of the NPs. The XRD patterns obtained for the Ni NPs samples with various precursors are shown in Figure 18. It can be seen that all diffractograms present the characteristic peaks for Ni^0 phase. The major difference noticed between the precursors is the intensity of the peaks, related with the average particle sizes obtained. At a reaction time of 20 h, $Ni(Ac)_2$ (Ac-CH_3COO) precursor showed a highly intense peak, which can be explained by the size of NPs obtained from the precursor at the said conditions (Figure 19). Indeed, an

increase in particle size reduces the broadness of the peak which could translate to a nonuniform dispersion if incorporated on a support. Furthermore, at 12 h reaction time, the particle sizes for all the different precursors showed hardly any variation amongst themselves and had a size range between 17.4 – 17.9 nm.

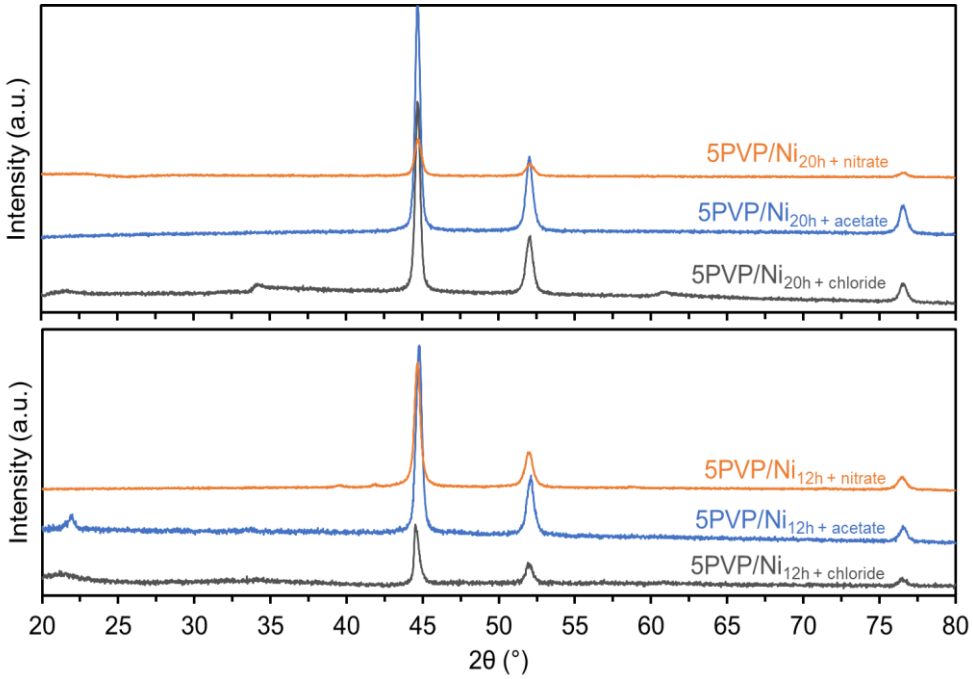

Figure 18: XRD patterns for Ni NP samples with different precursors at 12 and 20 h reaction time.

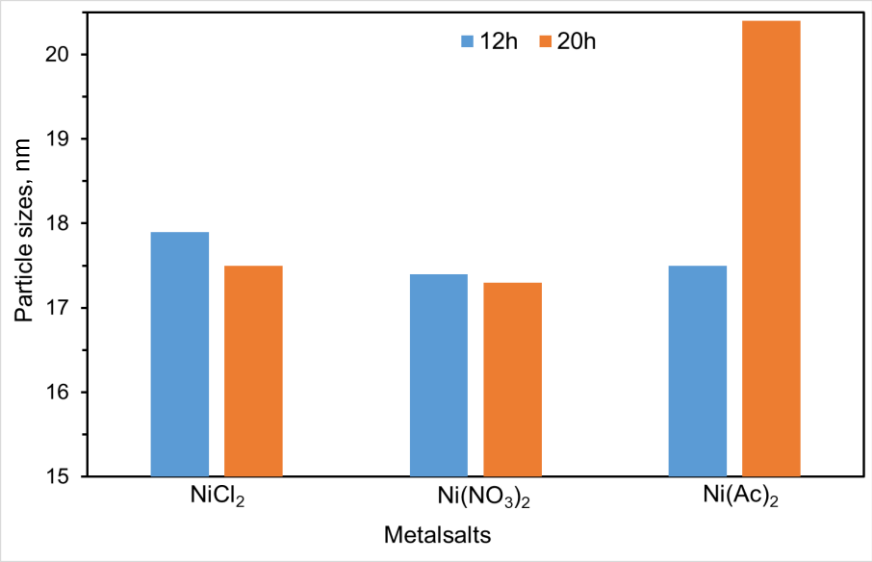

Figure 19: Nickel NPs sizes against metal precursors at reaction time of 12 and 24 h.

Overall, considering the results obtained, a conclusion was reached based on the above analyzed key-points and the most suitable conditions to further study the process for the synthesis of Ni-based catalysts over zeolite supports were selected to be the following: i) PVP/Ni ratio: 5; ii) Reaction time: 12 h and 20 h (at 180 ºC). and iii) Precursor salt: $NiCl_2$.

3.2 Study of Ni-based zeolite-supported catalysts

Taking into account the best solvothermal method conditions for the synthesis of Ni NPs defined in the previous chapter, a series of Ni and Ru-zeolite catalysts were prepared, characterized and tested for CO_2 methanation.

To start, four Ni/USY catalysts were synthesized using 12 and 20 h of reaction time and two types of zeolites with variable compensating cations: H^+ (HUSY, acidic and hydrophilic zeolite) and Cs^+ (CsUSY, more basic and hydrophobic zeolite). The XRD patterns of the four Ni/USY catalyst samples are shown in Figure 20. As noticed, it can be seen that there are no intense nor clear peaks in the diffractogram, which suggests that the metal species could be highly dispersed in the zeolite. Complementary, the lack of zeolite characteristic peaks in the metal-containing catalysts indicates the destruction of the zeolite structure [68].

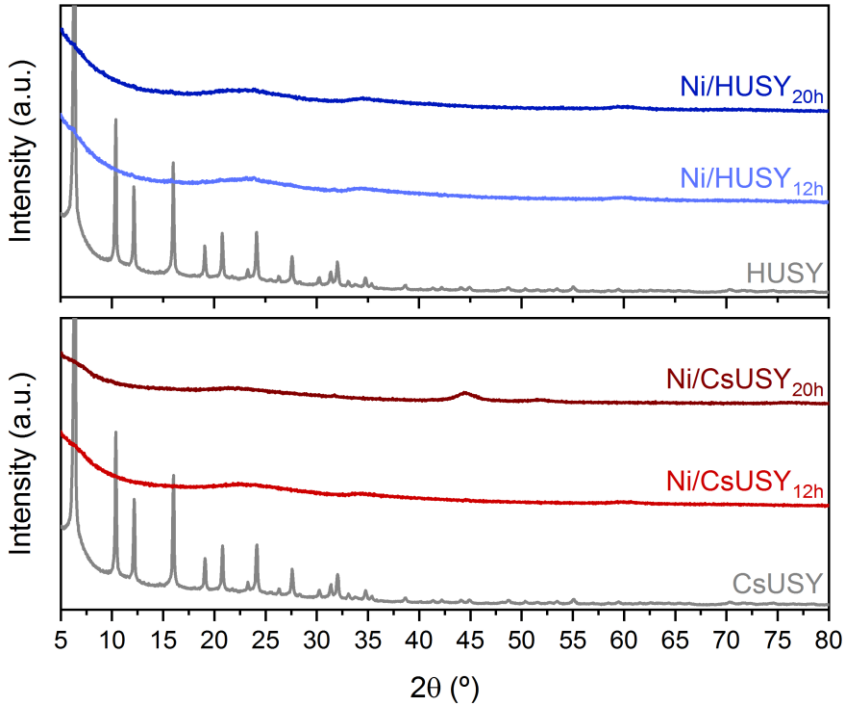

Figure 20: XRD pattern of Ni/USY catalyst samples prepared at 12 and 20 h reaction time.

Regarding the BET surface area of the catalysts (S_{BET}), the results are presented in Table 6.

Table 6: BET surface area of Ni/USY catalyst samples prepared at 12 and 20 h reaction time.

Catalyst	Surface area (m^2/g)
HUSY	450
Ni/HUSY$_{12h}$	8.8
Ni/HUSY$_{20h}$	8.5
CsUSY	579
Ni/CsUSY$_{12h}$	59
Ni/CsUSY$_{20h}$	13

According to Abu Bakar *et al.* [69], the BET surface area is presumed to be reduced when there is no generation of new active sites. Catalyst's S_{BET} values were significantly lower than those found for the HUSY and CsUSY supports, which could be due to the damage of the zeolite structure and/or to the presence of precursor salt in the samples. Also, it can be noted that catalyst samples prepared at shorter reaction time (12 h) have higher surface areas, being this effect more evident in the CsUSY series.

To further investigate, the catalyst samples prepared using a reaction time of 12 h were characterized by H_2-TPR (Figure 21). As verified, negative peaks were revealed by both catalysts, which confirm the earlier hypothesis regarding the presence of a part of the precursor salt remaining in the samples even after the synthesis procedure, considering that any heat treatment was performed.

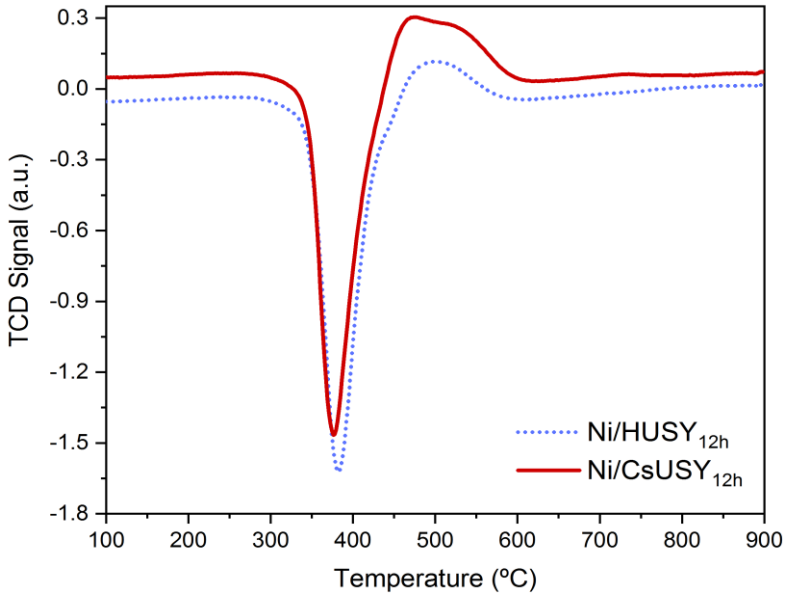

Figure 21: H_2-TPR profiles of Ni/USY catalysts at 12 h reaction time.

Furthermore, in terms of catalytic performances, CO_2 conversion and CH_4 selectivity, are presented in Figure 22.

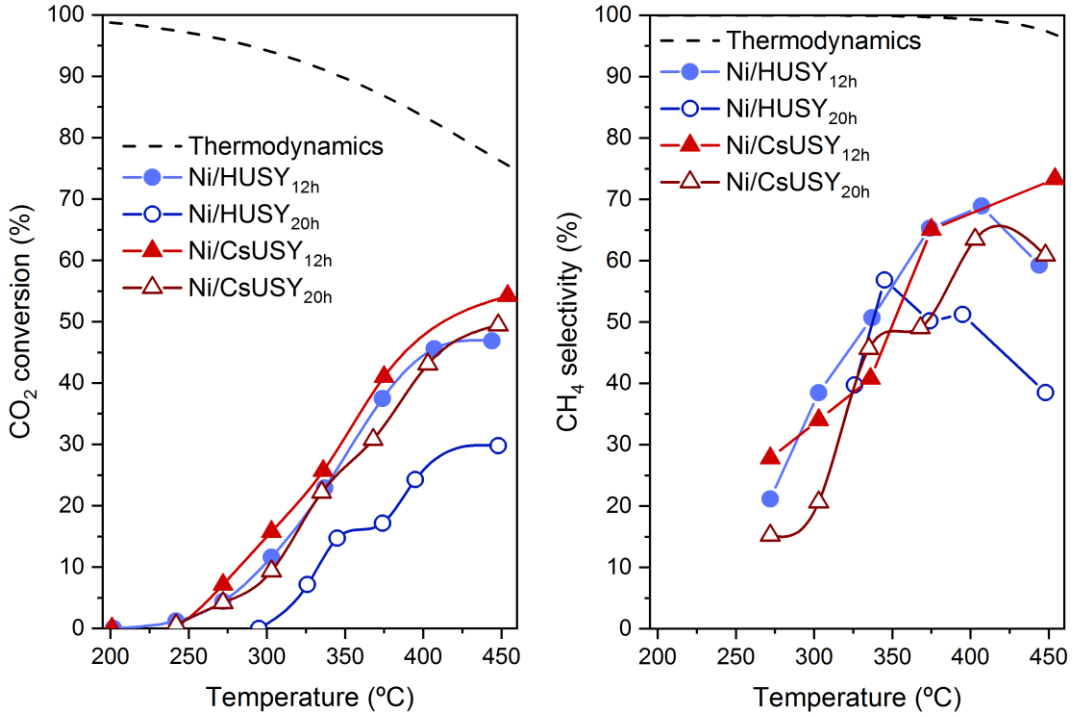

Figure 22: CO_2 conversion and CH_4 selectivity vs. reaction temperature for the Ni/HUSY and Ni/CsUSY catalysts prepared using 12 h and 20 h of reaction time. Conditions: reduction at 470 ºC, H_2:CO_2:N_2=36:9:10, 87000 ml h^{-1} g^{-1}. Dashed line corresponds to thermodynamic equilibrium values.

Starting by the analysis of the reaction time effect, lower activities were observed for the catalysts prepared at 20 h as compared with 12 h reaction time in both the HUSY and CsUSY supported catalysts. This effect could be ascribed to the formation of larger Ni particle. However, there is a more pronounced difference between the activities of Ni/HUSY catalyst samples, an effect that could be related to the nature of the zeolite. Indeed, in the literature it was reported that Ni/USY zeolites containing larger compensating cations (Cs^+) can partially suppress metal agglomeration processes, increasing the resistance towards sintering [70], [71]. Consequently, Ni/HUSY zeolites are expected to present lower resistance towards sintering processes induced by, for instance, higher reaction times. In terms of zeolite nature effect, both for 12 and 20 h of reaction time, it can be noted that Ni/CsUSY catalysts led to better performances than Ni/HUSY samples. These results could be ascribed, according to the literature [54], [70], to the influence of the zeolite's compensating cation (H^+ or Cs^+) in the basicity (higher in the case of CsUSY and responsible for an improvement of the CO_2 adsorption/activation) and the hydrophobicity (higher in the CsUSY and able to reduce the inhibitory effect of water in the reaction).

Considering that H_2-TPR revealed that part of the precursor salt might be present in the samples, the best materials ($Ni/HUSY_{12h}$ and $Ni/CsUSY_{12h}$) were calcined in a muffle for 2 h at 500 ºC using a heating rate of 1 ºC/min under atmospheric air and their H_2-TPR profiles were again collected (Figure 23). It was expected that the calcination treatment will help to convert any remaining precursor salts on the support into NiO. Calcined samples present main reduction processes below 650 ºC, which might be ascribed to the reduction of NiO species formed over the materials. The reducibility was clearly influenced by the nature of the zeolite support, with the HUSY leading to stronger Ni-support interactions (reduction processes occurring at higher temperatures).

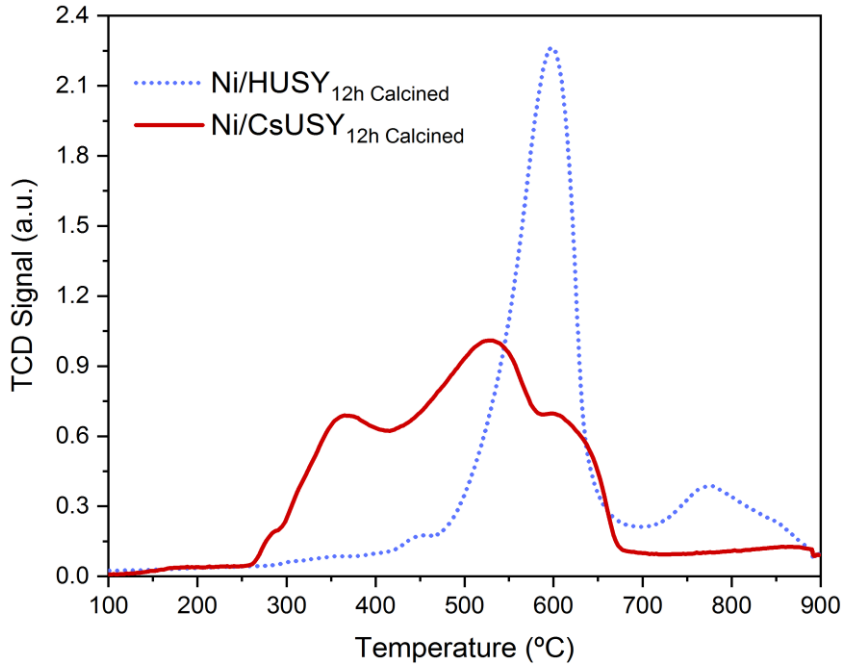

Figure 23: H_2-TPR profiles of calcined Ni/USY catalysts at 12 h reaction time.

XRD was also performed for these samples with the diffractograms shown in the Figure 24. Like the uncalcined samples, the Ni/USY calcined catalysts had no clear diffraction peaks attributed to the NiO/Ni^0 phases.

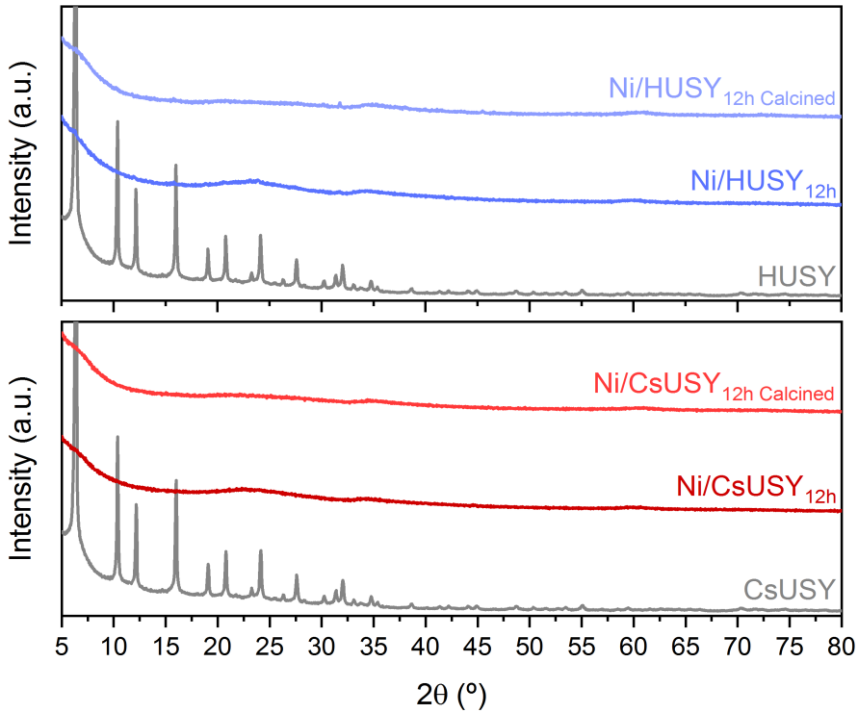

Figure 24: XRD pattern of calcined Ni/USY catalyst samples prepared at 12 h reaction time.

Regarding BET analysis of the calcined Ni/USY samples, a considerable increase in the samples' S_{BET} was observed after the heating treatment, which confirm the removal of the precursor salt from the materials. This could result in an increased number of active sites in the catalysts, which may contribute to increase their catalytic activity [69].

Table 7: BET surface area of calcined and uncalcined Ni/USY catalyst samples prepared at 12 h reaction time.

Catalyst	Surface area (m^2/g)
$Ni/HUSY_{12h}$	8.8
$Ni/HUSY_{12h\ Calcined}$	161
$Ni/CsUSY_{12h}$	59
$Ni/CsUSY_{12h\ Calcined}$	135

Catalytic tests were run over the calcined materials and the results are presented in Figure 25. As seen from the graph, CO_2 conversions and CH_4 selectivity were higher in the uncalcined samples. This unexpected behavior could be related to the negative effect of carrying out two thermal treatments at high temperature (calcination at 500 ºC and pre-reduction at 470 ºC) in the agglomeration of Ni particles for the case of the calcined samples. Consequently, despite the presence of precursor salt in the uncalcined samples, the pre-reduction treatment at 470 ºC could be enough for obtaining well-dispersed Ni^0 nanoparticles leading to a higher CH_4 yield.

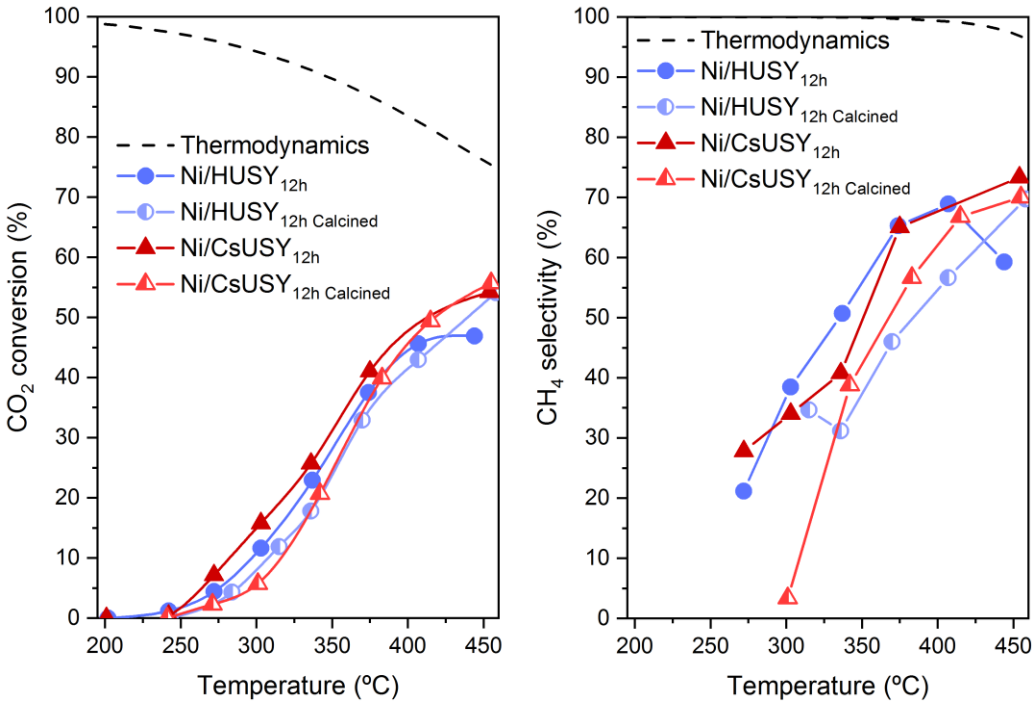

Figure 25: Comparison of calcined and uncalcined Ni/USY catalysts in terms of CO_2 conversion and CH_4 selectivity vs. reaction temperature. Conditions: reduction at 470 ºC, H_2:CO_2:N_2=36:9:10, 87000 ml h^{-1} g^{-1}. Dashed line corresponds to thermodynamic equilibrium values.

In order to verify the best type of zeolite support, CH_4 yields were determined (Figure 26). Although CO_2 methanation is favorable thermodynamically at low temperature, achieving the complete conversion of CO_2 into CH_4 at a relatively low temperature is challenging because of the difficult CO_2 activation process and the slow reaction kinetics at low temperatures [72].

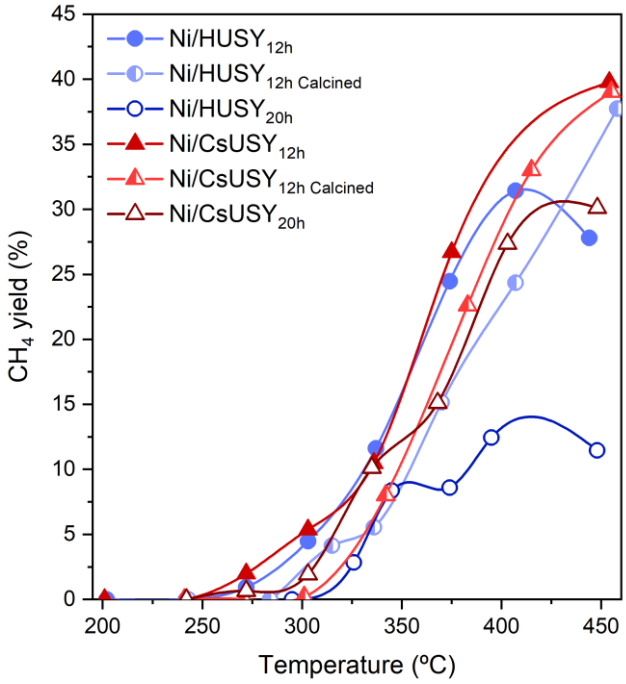

Figure 26: Comparison of different Ni/Zeolite samples prepared by solvothermal method in terms of CH4 yield vs. reaction temperature. Conditions: reduction at 470 ºC, H2:CO2:N2=36:9:10, 87000 ml h-1 g-1. Dashed line corresponds to thermodynamic equilibrium values.

As shown on the graph, CH_4 yields were highly far from the equilibrium points for all the solvothermal samples. The CH_4 yield for the catalyst samples mostly occurred from temperature above 300 ºC and the highest CH_4 yields were obtained at above 400ºC. As previously discussed, catalysts prepared by solvothermal during 20 h had the lowest CH_4 yield, which can be due to the longer reaction time causing the sintering of the catalysts and/or carbon deposition on the catalyst's active sites [45] as well as reducing its surface area (Table 7). Also, calcination did not favor in a significant manner the catalytic performances, probably due to the promotion of Ni particles aggregation due to the two thermal treatments carried out prior to the test. Overall, CsUSY-based catalysts, namely $Ni/CsUSY_{12h}$, exhibited the most promising results.

Furthermore, and taking into account Abu Bakar *et al.* [69] work suggesting that catalyst's preparation method may have an impact on how metallic Ni NPs is dispersed on the support, $Ni/HUSY_{12h}$ and $Ni/CsUSY_{12h}$ catalysts results were compared with those obtained for reference catalysts prepared by incipient wetness impregnation method [54], [73] (Figure 27). As seen, impregnation samples led to a significantly higher CH_4 yield, which could be due to the fact that zeolite structure was preserved in the impregnated samples [73]. Interestingly, whatever the preparation method, better results were obtained over the CsUSY zeolite catalysts, asserting on the suitability of using basic and hydrophobic supports.

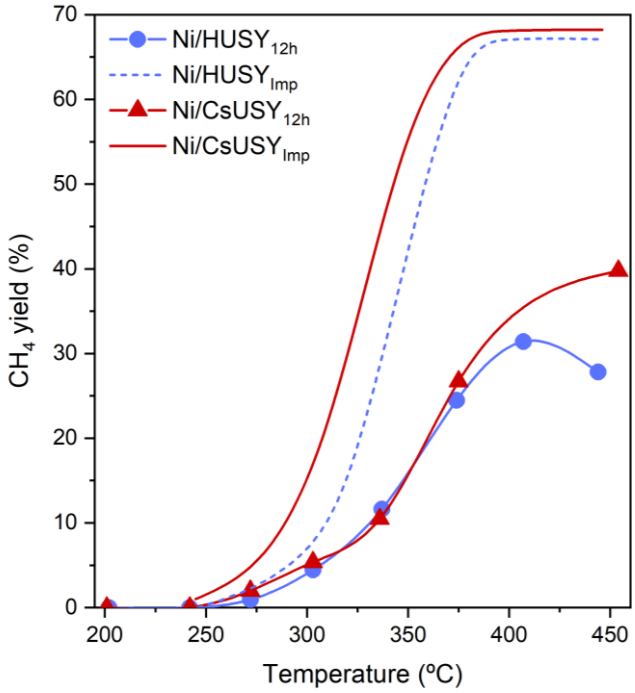

Figure 27: Comparison of different Ni/Zeolite catalysts prepared by solvothermal and impregnation methods in terms of CH_4 yield in temperature. Conditions: reduction at 470 ºC, H_2:CO_2:N_2=36:9:10, 87000 ml h^{-1} g^{-1}. Dashed line corresponds to thermodynamic equilibrium values.

As previously discussed, Ni-based CsUSY catalysts lead to better catalytic performances. However, with the aim of identifying if the destruction of the zeolite structure observed by XRD could be in the origin of the low performances revealed by solvothermal samples, two mechanical mixtures of CsUSY zeolite and Ni NPs synthesized using 12 and 20 h of reaction time were prepared, characterized by XRD and tested towards CO_2 methanation without a pre-reduction step (as Ni will be already in metallic form in these materials). Starting by the analysis of the XRD patterns (Figure 28), clear diffraction peaks attributed to the zeolite structure (5-45 º region) can be observed, while the presence of Ni NPs is also noted.

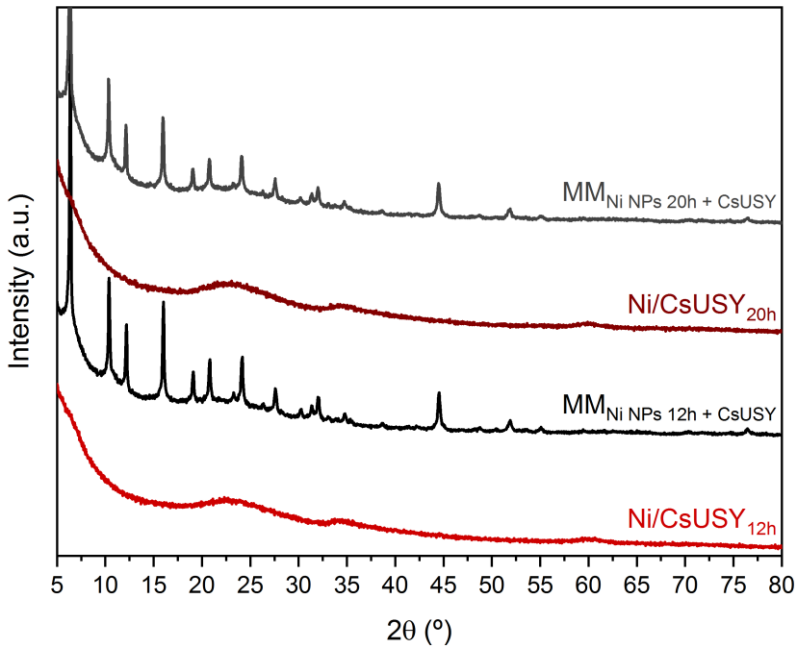

Figure 28: XRD pattern for mechanical mixtures and Ni/CsUSY samples (at 12 and 20 h reaction time).

In terms of catalytic performances of mechanical mixtures (Figure 29), the results obtained showed a much lower CO_2 conversion and selectivity to CH_4 than those revealed by the solvothermal samples. This indicates that, despite the destruction of the zeolite structure, a favorable metal-support interaction might be established during the solvothermal procedure, presenting a positive influence in the samples' properties [52].

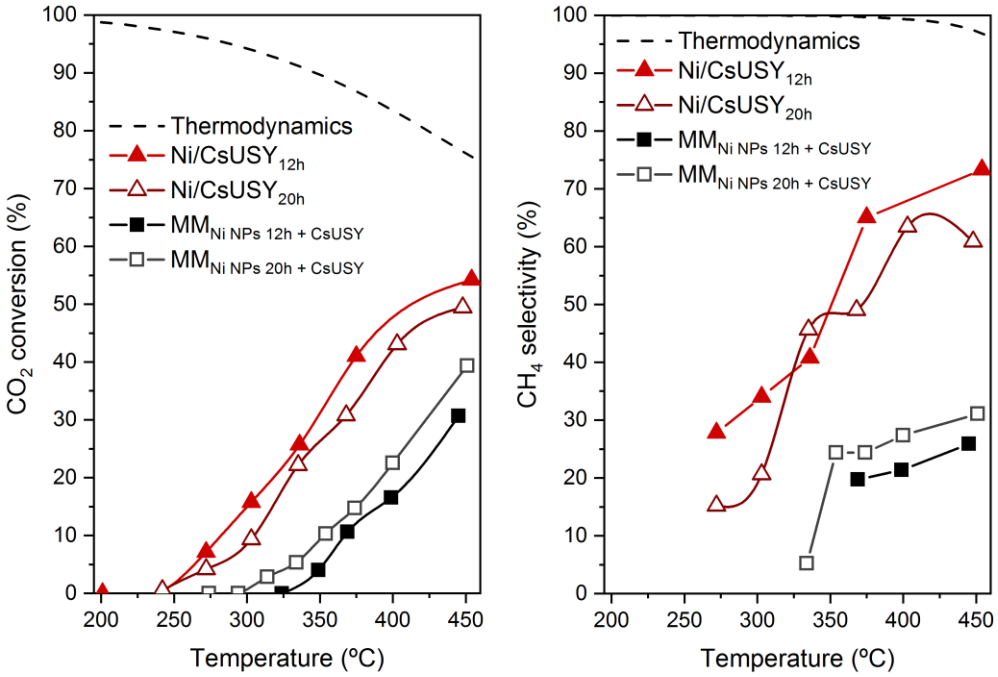

Figure 29: Comparison of the catalytic performances of mechanical mixtures and solvothermal catalysts. Conditions: reduction at 470 ºC, H_2:CO_2:N_2=36:9:10, 87000 ml h^{-1} g^{-1}. Dashed line corresponds to thermodynamic equilibrium values.

3.3 Study of the metal nature effect

Moreover, and with the objective of identifying the effect of the active metal nature, the best sample ($Ni/CsUSY_{12h}$), was compared to a 3 wt.% Ru catalyst ($Ru/CsUSY_{12h}$, Ru loading optimized in previous research studies at CATHPRO/CQE group carried out using incipient wetness impregnation as a preparation method). As seen in Figure 30 and contrary to what found for $Ni/CsUSY_{12h}$ sample, $Ru/CsUSY_{12h}$ pattern exhibits the diffraction peaks attributed to the zeolite structure. This fact can be due to the non-required utilization of NaOH for the pH adjustment during the Ru nanoparticles synthesis process, which might be related to the lower metal loading used (3 wt.% Ru vs 15 wt.% in the case of Ni catalysts). Also, no diffraction peaks attributed to RuO_2/Ru^0 can be found, most likely due to the low metal loading and/or the high dispersion on the zeolite. [69].

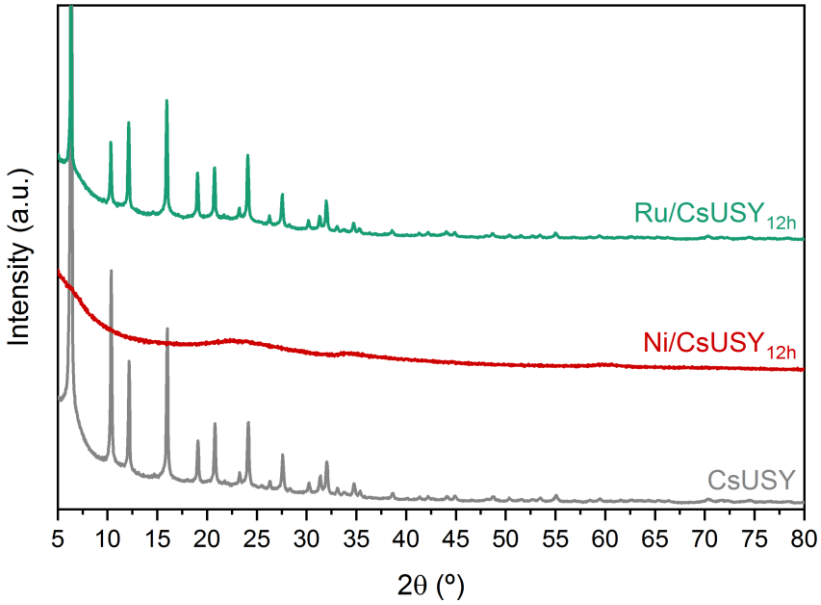

Figure 30: XRD pattern for Ni and Ru solvothermal samples (at 12 reaction time).

In terms of catalytic performances (Figure 31), with $Ni/CsUSY_{12h}$ catalyst the CO_2 conversions are higher, while the use of Ru significantly favored CH_4 selectivity, in accordance with the other studies [57], [72]. Complementary, the CH_4 yield over $Ru/CsUSY_{12h}$ catalyst was higher than the obtained for the $Ni/CsUSY_{12h}$ above ~425 ℃. These results indicate that Ru loading and pre-reduction temperature must be optimized in solvothermal Ru-samples, as the 3 wt.% Ru (best Ru loading) and 200 ºC (best pre-reduction temperature) arising from impregnation studies could not be the most appropriate when changing the synthesis method.

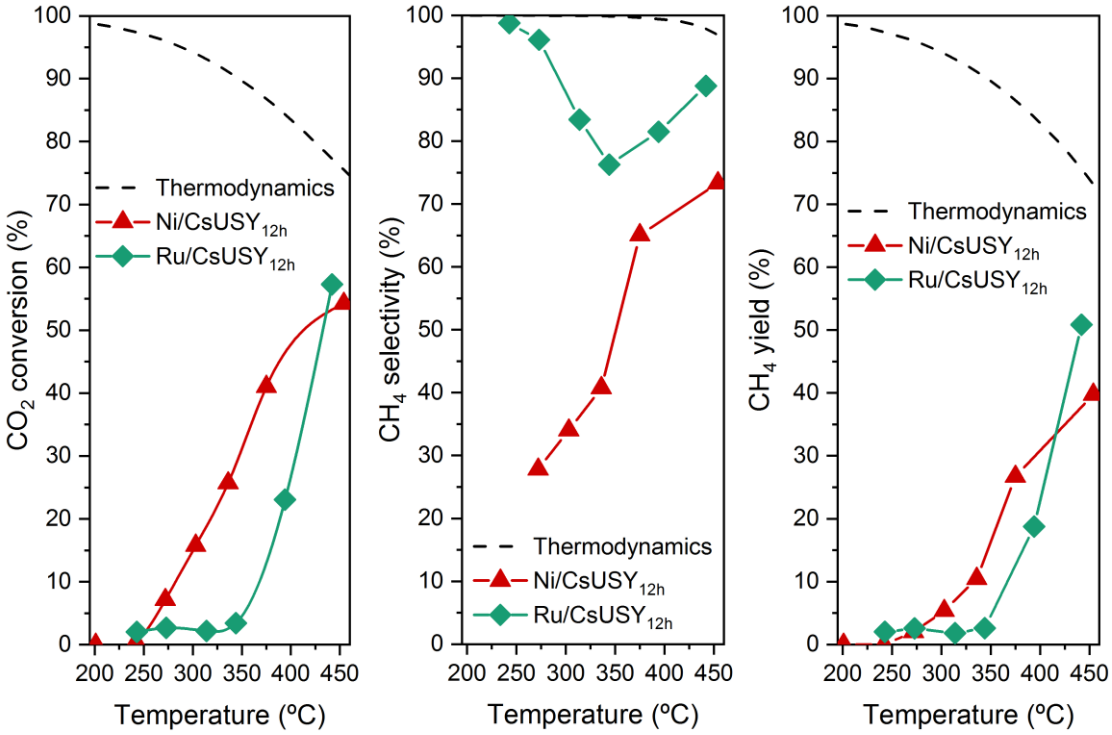

Figure 31: Comparison of the performance of Ru/CsUSY with Ni/CsUSY. Conditions: reduction at 470 ºC (Ni samples) and 200 ºC (Ru samples), H2:CO2:N2=36:9:10, 87000 ml h-1 g-1. Dashed line corresponds to thermodynamic equilibrium values.

Complementary, the effects of the preparation method were analyzed by comparing solvothermal and impregnated catalysts performances in terms of CH_4 yields (Figure 32). In accordance with the previous findings regarding Ni/Zeolite solvothermal samples, impregnation was found as a more appropriate method.

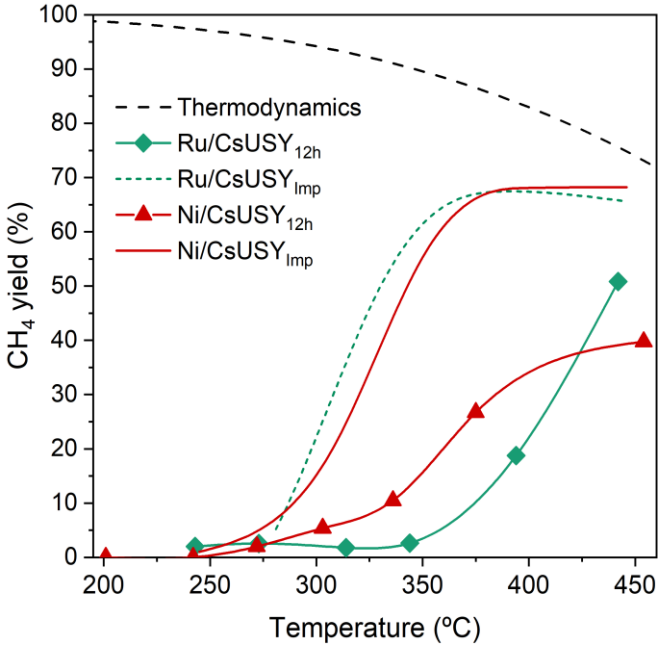

Figure 32: Comparison of the performance of Ru/CsUSY with Ni/CsUSY prepared by both solvothermal and impregnation methods. Conditions: reduction at 470 ºC (Ni samples) and 200 ºC (Ru samples), H_2:CO_2:N_2=36:9:10, 87000 ml h^{-1} g^{-1}. Dashed line corresponds to thermodynamic equilibrium values.

3.4 Spent samples characterization

Finally, all samples were analyzed after catalytic reaction (spent) by XRD. For the HUSY-based catalysts (Figure 33), diffraction peaks were observed at 2θ values of 44.5° and 52.1°, which can be attributed to the presence of metallic nickel in the samples. This confirms that the catalyst's pre-reduction treatment allowed the formation of Ni^0 particles, irrespective of the existence of a previous calcination step or not. Also, the diffraction peaks are noticeably broad, caused by very small NPs which signify a high dispersion of metallic Ni on the support [69].

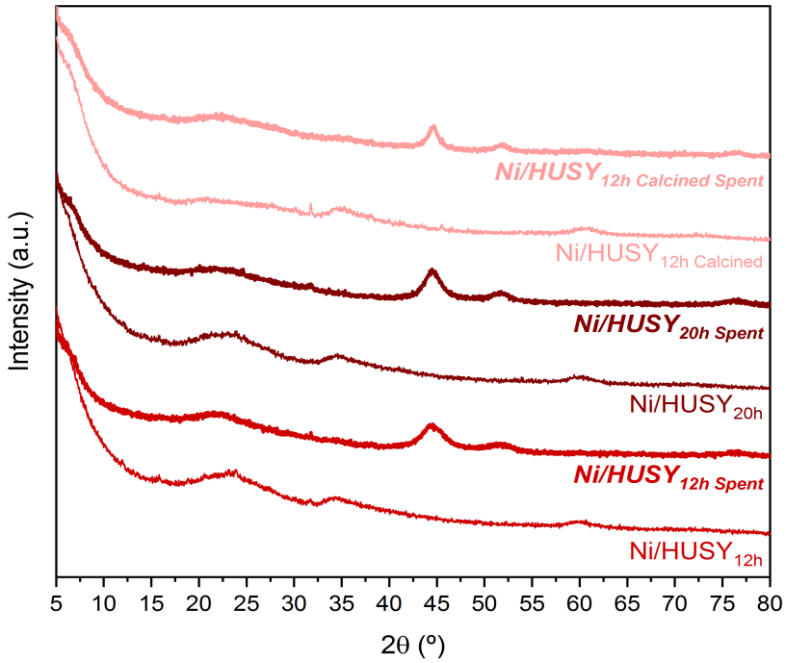

Figure 33: XRD pattern for the fresh and spent Ni/USY samples (at 12 and 20 h reaction time).

Relatively to the CsUSY-supported catalysts (Figure 34), similar observations can be verified both for the samples without (A) or with (B) zeolite diffraction peaks under fresh conditions.

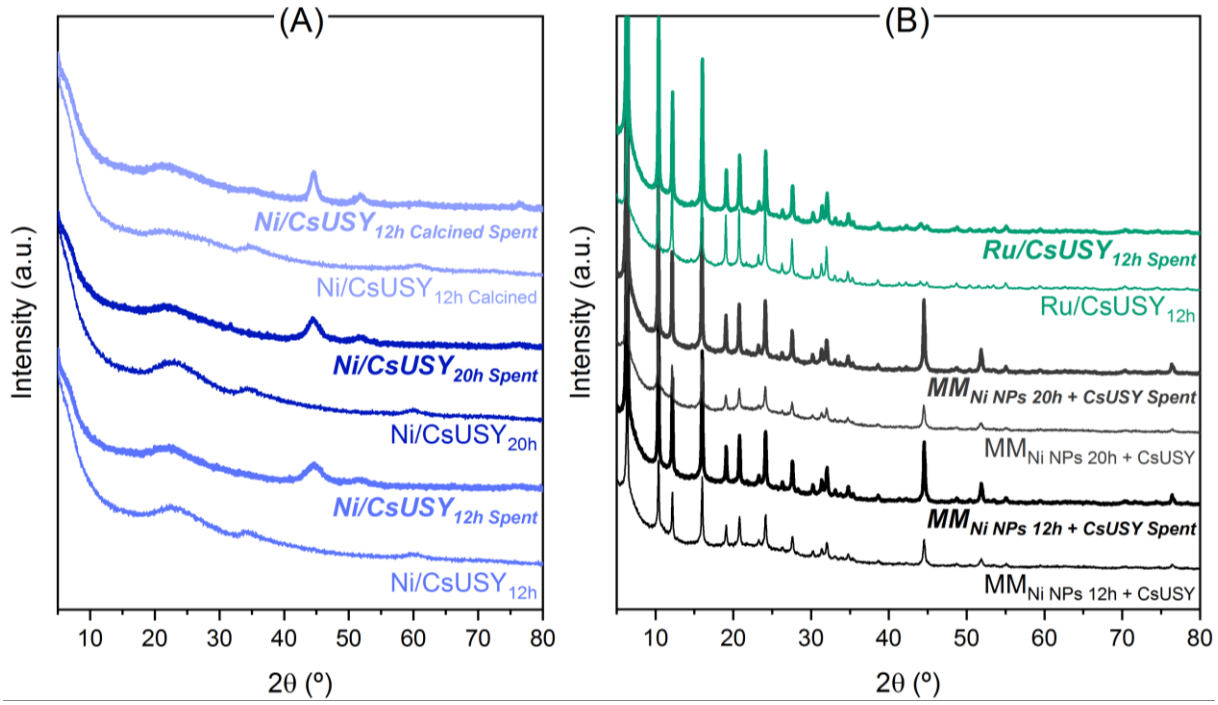

Figure 34: XRD pattern for (A) Ni/CsUSY solvothermal samples (at 12 and 20 h reaction time) and (B) mechanical mixtures and Ru/CsUSY12h catalysts under fresh and spent conditions.

The observed diffraction peaks corresponding to metallic Ni phase that can be found in all spent Ni catalysts. Regarding the Ni/CsUSY samples series (Figure 34 A), one can see that metallic nickel diffraction peaks become sharper with the increase of the reaction time and even with the calcination treatment that can be correlate with the nickel particle size and also with catalytic activity observed ($Ni/CsUSY_{12h\ Calcined}$ < $Ni/CsUSY_{20h}$ < $Ni/CsUSY_{12h}$). Analyzing the patterns obtained for the mechanical mixtures (MM, Figure 34 B), it is clear the increased intensity of the Ni^0 diffraction peaks after tests. This indicates the occurrence of particles agglomeration/sintering during the reaction, probably due to the lack of metal-support interactions able to hinder these processes in these catalysts. This observation contributes to the previous explanation to the low performances registered for the MM samples. Finally, no remarkable differences can be found when comparing the patterns obtained for $Ru/CsUSY_{12h}$ sample before or after the test.

4. Conclusions and Future Work

CO_2 methanation can be considered as a promising alternative for upgrading biogas into biomethane as it allows the maximization of the renewable carbon valorization. Among the different methanation catalysts found in the literature, the use of zeolites has led to interesting results so far. However, the considerably large Ni^0 particles obtained in absence of promoters (25-30 nm) and by conventional impregnation method are one of their main drawbacks.

In this context, the present research project aimed to investigate the preparation of Ni/USY catalysts by using solvothermal method, a low energy intensive process. The influence of the reaction time, PVP/Ni ratio and Ni metal precursor in the Ni NPs size were evaluated and properly optimized, in order to use the best conditions in the preparation of metal-based zeolite catalysts.

As expected, using high PVP/Ni ratio allowed the formation of Ni^0 particles with sizes lower than 20 nm while high reaction time did not significantly impact the NPs sizes. Complementary, the nature of the Ni precursor salt led to a slight impact in the results, when the samples prepared at 12 h were compared (reaction time) and a higher impact when the samples were prepared at 20 h. Based on the results obtained, the most favorable conditions for the preparation of Ni and Ru-based USY catalysts were established to be 12 and 20 h with PVP/Ni ratio of 5, using the chloride salts.

Regarding the zeolite-containing samples, the use of 12 h as reaction time was responsible for higher catalytic performances. Complementary, the choice of a basic and hydrophobic zeolite (CsUSY) was found as more promising. Despite the verified destruction of the zeolite structure during the synthesis procedure, probably due to the required addition of NaOH in the protocol for the pH adjustment, favorable metal-support interactions might be established during the solvothermal procedure, as mechanical mixtures of CsUSY and Ni NPs led to lower performances and evident metallic sintering. Finally, no improvements were verified when using Ru instead of Ni as active method, probably due to the differences in terms of metal loadings. Overall, solvothermal samples showed moderate potential towards CO_2 methanation, especially when comparing with equivalent samples prepared by impregnation method where the zeolite structure was preserved. however, the produced catalyst still requires tangible improvement to obtain significant CO_2 conversion and selectivity to CH_4.

On the other hand, the comparison of Ru-based catalyst, which is a very good active metal for methanation, with the Ni-based showed a slightly better result. The characterization of the Ru/CsUSY catalyst showed the presence of zeolite structure diffraction peaks which means the structure was unaffected as in the case of Ni/USY samples.

In conclusion, the results obtained in this work showed that further efforts must be done for improving the performances of Ni/zeolite catalysts synthesized by solvothermal method. To optimize the synthesis process and achieve better results, this work should be extended to varying other parameters including % of Ni loading, different calcination temperature and use promoters in order to improve the metal particle size and dispersion as well as study their effect on catalytic behavior.

Bibliography

[1] M. Abrantes, F. Lemos, and M. A. Lemos, 'Alternative Fuels. World Energy Overview'. 2018.

[2] H. Ritchie and M. Roser, 'Energy', *Our World in Data*, Mar. 2014, Accessed: Apr. 29, 2020. [Online]. Available: https://ourworldindata.org/energy.

[3] 'Statistical Review of World Energy | Energy economics | Home', *BP global*. https://www.bp.com/en/global/corporate/energy-economics/statistical-review-of-world-energy.html (accessed Apr. 29, 2020).

[4] R. Heede, 'Tracing anthropogenic carbon dioxide and methane emissions to fossil fuel and cement producers, 1854–2010', *Climatic Change*, vol. 122, no. 1, pp. 229–241, Jan. 2014.

[5] 'Emissions – Global Energy & CO2 Status Report 2019 – Analysis', *IEA*. https://www.iea.org/reports/global-energy-co2-status-report-2019/emissions (accessed Apr. 29, 2020).

[6] 'Gas Flaring in Iraq', Feb. 22, 2014. https://earthobservatory.nasa.gov/images/83178/gas-flaring-in-iraq (accessed Apr. 29, 2020).

[7] 'REthinking Energy: Renewable Energy and Climate Change', */publications/2015/Nov/REthinking-Energy-Renewable-Energy-and-Climate-Change*. /publications/2015/Nov/REthinking-Energy-Renewable-Energy-and-Climate-Change (accessed Apr. 29, 2020).

[8] 'REthinking Energy 2017: Accelerating the global energy transformation', */publications/2017/Jan/REthinking-Energy-2017-Accelerating-the-global-energy-transformation*. /publications/2017/Jan/REthinking-Energy-2017-Accelerating-the-global-energy-transformation (accessed Apr. 29, 2020).

[9] P. A. Owusu and S. Asumadu-Sarkodie, 'A review of renewable energy sources, sustainability issues and climate change mitigation', *Cogent Engineering*, vol. 3, no. 1, p. 1167990, Dec. 2016.

[10] O. Ellabban, H. Abu-Rub, and F. Blaabjerg, 'Renewable energy resources: Current status, future prospects and their enabling technology', *Renewable and Sustainable Energy Reviews*, vol. 39, pp. 748–764, Nov. 2014.

[11] G. Luderer *et al.*, 'The role of renewable energy in climate stabilization: results from the EMF27 scenarios', *Climatic Change*, vol. 123, no. 3, pp. 427–441, Apr. 2014.

[12] D. Zhu, S. M. Mortazavi, A. Maleki, A. Aslani, and H. Yousefi, 'Analysis of the robustness of energy supply in Japan: Role of renewable energy', *Energy Reports*, vol. 6, pp. 378–391, Nov. 2020.

[13] J. S. Tumuluru, C. Wright, K. Kenny, and J. Hess, 'A Review on Biomass Densification for Energy Applications', May 2011.

[14] C. Loha, M. K. Karmakar, H. Chattopadhyay, and G. Majumdar, 'Renewable Biomass: A Candidate for Mitigating Global Warming', in *Encyclopedia of Renewable and Sustainable Materials*, S. Hashmi and I. A. Choudhury, Eds. Oxford: Elsevier, 2020, pp. 715–727.

[15] L. E. N. Ekpeni, K. Y. Benyounis, F. Nkem-Ekpeni, J. Stokes, and A. G. Olabi, 'Energy Diversity through Renewable Energy Source (RES) – A Case Study of Biomass', *Energy Procedia*, vol. 61, pp. 1740–1747, Jan. 2014.

[16] T. A. Mamvura and G. Danha, ‘Biomass torrefaction as an emerging technology to aid in energy production’, *Heliyon*, vol. 6, no. 3, p. e03531, Mar. 2020.

[17] J. Ren, Y.-L. Liu, X.-Y. Zhao, and J.-P. Cao, ‘Methanation of syngas from biomass gasification: An overview’, *International Journal of Hydrogen Energy*, vol. 45, no. 7, pp. 4223–4243, Feb. 2020.

[18] V. Dhyani and T. Bhaskar, ‘A comprehensive review on the pyrolysis of lignocellulosic biomass’, *Renewable Energy*, vol. 129, pp. 695–716, Dec. 2018.

[19] P. Bajpai, ‘Chapter 5 - Biomass conversion processes’, in *Biomass to Energy Conversion Technologies*, P. Bajpai, Ed. Elsevier, 2020, pp. 41–151.

[20] F. Lü, Z. Hua, L. Shao, and P. He, ‘Loop bioenergy production and carbon sequestration of polymeric waste by integrating biochemical and thermochemical conversion processes: A conceptual framework and recent advances’, *Renewable Energy*, vol. 124, pp. 202–211, Aug. 2018.

[21] B. Shamurad *et al.*, ‘Stable biogas production from single-stage anaerobic digestion of food waste’, *Applied Energy*, vol. 263, p. 114609, Apr. 2020.

[22] J. Chen *et al.*, ‘Role of biomass-derived carbon-based composite accelerants in enhanced anaerobic digestion: Focusing on biogas yield, fertilizer utilization, and density functional theory calculations’, *Bioresource Technology*, vol. 307, p. 123204, Jul. 2020.

[23] A. Messineo, M. P. Maniscalco, and R. Volpe, ‘Biomethane recovery from olive mill residues through anaerobic digestion: A review of the state-of-the-art technology’, *Science of The Total Environment*, vol. 703, p. 135508, Feb. 2020.

[24] A. C. Wilkie, ‘Biomethane from Biomass, Biowaste, and Biofuels’, *Bioenergy*, pp. 195–205, Jan. 2008.

[25] ‘Potentialities of a dense skin hollow fiber membrane contactor for biogas purification by pressurized water absorption - ScienceDirect’. https://www.sciencedirect.com/science/article/abs/pii/S0376738816302587 (accessed May 08, 2020).

[26] K. Moustakas, P. Parmaxidou, and S. Vakalis, ‘Anaerobic digestion for energy production from agricultural biomass waste in Greece: Capacity assessment for the region of Thessaly’, *Energy*, vol. 191, p. 116556, Jan. 2020.

[27] J. Čermáková, J. Mrázek, K. Fliegerová, and D. Tenkrát, ‘Replacing natural gas by biogas - determining the bacterial contamination of biogas by PCR’, *Acta Polytechnica*, vol. 52, pp. 33–38, Jan. 2012.

[28] J. Haider, M. A. Qyyum, B. Kazmi, M. Zahoor, and M. Lee, ‘Simulation study of biomethane liquefaction followed by biogas upgrading using an imidazolium-based cationic ionic liquid’, *Journal of Cleaner Production*, vol. 231, pp. 953–962, Sep. 2019.

[29] S. Frigo and G. Spazzafumo, ‘Cogeneration of power and substitute of natural gas using biomass and electrolytic hydrogen’, *International Journal of Hydrogen Energy*, vol. 43, no. 26, pp. 11696–11705, Jun. 2018.

[30] M. Prussi, M. Padella, M. Conton, E. D. Postma, and L. Lonza, ‘Review of technologies for biomethane production and assessment of Eu transport share in 2030’, *Journal of Cleaner Production*, vol. 222, pp. 565–572, Jun. 2019.

[31] A. I. Adnan, M. Y. Ong, S. Nomanbhay, K. W. Chew, and P. L. Show, ‘Technologies for Biogas Upgrading to Biomethane: A Review’, *Bioengineering*, vol. 6, no. 4, Art. no. 4, Dec. 2019.

[32] K. Starr, G. Villalba, and X. Gabarrell, ‘Upgraded biogas from municipal solid waste for natural gas substitution and CO2 reduction – A case study of Austria, Italy, and Spain’, *Waste Management*, vol. 38, pp. 105–116, Apr. 2015.

[33] E. Billig and D. Thrän, ‘Evaluation of biomethane technologies in Europe – Technical concepts under the scope of a Delphi-Survey embedded in a multi-criteria analysis’, *Energy*, vol. 114, pp. 1176–1186, Nov. 2016.

[34] ‘Biogas to Biomethane’. https://www.biogas-to-biomethane.com/Download/BTB.pdf (accessed May 09, 2020).

[35] I. Ullah Khan *et al.*, ‘Biogas as a renewable energy fuel – A review of biogas upgrading, utilisation and storage’, *Energy Conversion and Management*, vol. 150, pp. 277–294, Oct. 2017.

[36] T. Rattanaya, P. Kongjan, C. Bunyakan, A. Reungsang, and R. Jariyaboon, ‘Upgrading biogas to biomethane: Alkaline recovery of absorbed solution by thermal decomposition’, *Process Safety and Environmental Protection*, vol. 138, pp. 157–166, Jun. 2020.

[37] X. Y. Chen, H. Vinh-Thang, A. A. Ramirez, D. Rodrigue, and S. Kaliaguine, ‘Membrane gas separation technologies for biogas upgrading’, *RSC Adv.*, vol. 5, no. 31, pp. 24399–24448, Mar. 2015.

[38] L. A. Pellegrini, G. De Guido, and S. Langé, ‘Biogas to liquefied biomethane via cryogenic upgrading technologies’, *Renewable Energy*, vol. 124, pp. 75–83, Aug. 2018.

[39] T. Kvist and N. Aryal, ‘Methane loss from commercially operating biogas upgrading plants’, *Waste Management*, vol. 87, pp. 295–300, Mar. 2019.

[40] S. Sahota *et al.*, ‘Review of trends in biogas upgradation technologies and future perspectives’, *Bioresource Technology Reports*, vol. 1, pp. 79–88, Mar. 2018.

[41] B. Castellani, E. Morini, E. Bonamente, and F. Rossi, ‘Experimental investigation and energy considerations on hydrate-based biogas upgrading with CO2 valorization’, *Biomass and Bioenergy*, vol. 105, pp. 364–372, Oct. 2017.

[42] B. Castellani, S. Rinaldi, E. Bonamente, A. Nicolini, F. Rossi, and F. Cotana, ‘Carbon and energy footprint of the hydrate-based biogas upgrading process integrated with CO2 valorization’, *Science of The Total Environment*, vol. 615, pp. 404–411, Feb. 2018.

[43] R. R. Boggula, D. Fischer, R. Casaretto, and J. Born, ‘Methanation potential: Suitable catalyst and optimized process conditions for upgrading biogas to reach gas grid requirements’, *Biomass and Bioenergy*, vol. 133, p. 105447, Feb. 2020.

[44] G. Leonzio, ‘Process analysis of biological Sabatier reaction for bio-methane production’, *Chemical Engineering Journal*, vol. 290, pp. 490–498, Apr. 2016.

[45] M. M. Jaffar, M. A. Nahil, and P. T. Williams, ‘Parametric Study of CO2 Methanation for Synthetic Natural Gas Production’, *Energy Technology*, vol. 7, no. 11, p. 1900795, Aug. 2019.

[46] J. A. Hernandez Lalinde, P. Roongruangsree, J. Ilsemann, M. Bäumer, and J. Kopyscinski, ‘CO2 methanation and reverse water gas shift reaction. Kinetic study based on in situ spatially-resolved measurements’, *Chemical Engineering Journal*, vol. 390, p. 124629, Jun. 2020.

[47] P. Frontera, A. Macario, M. Ferraro, and P. Antonucci, ‘Supported Catalysts for CO2 Methanation: A Review’, *Catalysts*, vol. 7, no. 2, Art. no. 2, Feb. 2017.

[48] L. Falbo, M. Martinelli, C. G. Visconti, L. Lietti, C. Bassano, and P. Deiana, ‘Kinetics of CO2 methanation on a Ru-based catalyst at process conditions relevant for Power-to-Gas applications’, *Applied Catalysis B: Environmental*, vol. 225, pp. 354–363, Jun. 2018.

[49] A. Loder, M. Siebenhofer, and S. Lux, ‘The reaction kinetics of CO2 methanation on a bifunctional Ni/MgO catalyst’, *Journal of Industrial and Engineering Chemistry*, vol. 85, pp. 196–207, May 2020.

[50] F. Kosaka *et al.*, ‘Effect of Ni content on CO2 methanation performance with tubular-structured Ni-YSZ catalysts and optimization of catalytic activity for temperature management in the reactor’, *International Journal of Hydrogen Energy*, vol. 45, no. 23, pp. 12911–12920, Apr. 2020.

[51] G. Jiajian, G. Fangna, L. Qing, and L. Bin, ‘Recent Advances in Methanation Catalysts for the Production of Synthetic Natural Gas’, *ResearchGate*. https://www.researchgate.net/publication/272522542_Recent_Advances_in_Methanation_Catalysts_for_the_Production_of_Synthetic_Natural_Gas (accessed Aug. 28, 2020).

[52] I. Graça, L.V.González, M.C.Bacariza, A.Fernandes, C.Henriques, J.M.Lopes, and M.F.Ribeiro, ‘CO2 hydrogenation into CH4 on NiHNaUSY zeolites’, *Applied Catalysis B: Environmental*, vol. 147, pp. 101–110, Apr. 2014.

[53] M. a. A. Aziz, A. A. Jalil, S. Triwahyono, and A. Ahmad, ‘CO2 methanation over heterogeneous catalysts: recent progress and future prospects’, *Green Chem.*, vol. 17, no. 5, pp. 2647–2663, May 2015.

[54] M. C. Bacariza, I. Graça, J. M. Lopes, and C. Henriques, ‘Tuning Zeolite Properties towards CO2 Methanation: An Overview’, *ChemCatChem*, vol. 11, no. 10, pp. 2388–2400, May 2019.

[55] R. Alotaibi, F. Alenazey, F. Alotaibi, N. Wei, A. Al-Fatesh, and A. Fakeeha, ‘Ni catalysts with different promoters supported on zeolite for dry reforming of methane’, *Appl Petrochem Res*, vol. 5, no. 4, pp. 329–337, Dec. 2015.

[56] I. Sreedhar, Y. Varun, S. A. Singh, A. Venugopal, and B. M. Reddy, ‘Developmental trends in CO2 methanation using various catalysts’, *Catal. Sci. Technol.*, vol. 9, no. 17, pp. 4478–4504, Aug. 2019.

[57] A. Ricca, L. Truda, and V. Palma, ‘Study of the role of chemical support and structured carrier on the CO2 methanation reaction’, *Chemical Engineering Journal*, vol. 377, p. 120461, Dec. 2019.

[58] M. C. Bacariza, M. Maleval, I. Graça, J. M. Lopes, and C. Henriques, ‘Power-to-methane over Ni/zeolites: Influence of the framework type’, *Microporous and Mesoporous Materials*, vol. 274, pp. 102–112, Jan. 2019.

[59] P. Yu, B. Cui, Y. Zhang, and Q. Shi, ‘A Facile Solvothermal Synthesis of Monodisperse Ni Nanoparticles’, *Chemical Research in Chinese Universities*, vol. 24, no. 3, pp. 260–262, May 2008.

[60] A. Jentys and J. A. Lercher, ‘Chapter 8 Techniques of zeolite characterization’, in *Studies in Surface Science and Catalysis*, vol. 137, H. van Bekkum, E. M. Flanigen, P. A. Jacobs, and J. C. Jansen, Eds. Elsevier, 2001, pp. 345–386.

[61] ‘Characterization of Solid Materials and Heterogeneous Catalysts: From Structure to Surface Reactivity, 2 Volume Set | Wiley’, *Wiley.com*. https://www.wiley.com/en-us/Characterization+of+Solid+Materials+and+Heterogeneous+Catalysts%3A+From+Structure+to+Surface+Reactivity%2C+2+Volume+Set-p-9783527326877 (accessed Jun. 02, 2020).

[62] R. A. Schoonheydt, ‘Characterization of Solid Materials and Heterogeneous Catalysts. From Structure to Surface Reactivity. Edited by Michel Che and Jacques C. Védrine.’, *Angewandte Chemie International Edition*, vol. 51, no. 48, pp. 11938–11939, 2012.

[63] F. Pinna, ‘Supported metal catalysts preparation’, *Catalysis Today*, vol. 41, no. 1, pp. 129–137, May 1998.

[64] ‘CO2 conversion to CH4 using metallic catalysts supported on zeolites | Request PDF’, *ResearchGate*. https://www.researchgate.net/publication/327499573_CO2_conversion_to_CH4_using_metallic_catalysts_supported_on_zeolites (accessed Sep. 12, 2020).

[65] C. Lundstedt, ‘BET Theory and how its used to calculate surface area’, p. 19, 2018.

[66] ‘Silicon-carbon nanocomposite pyrolyzed from phenolic resin’, *ResearchGate*. https://www.researchgate.net/publication/310721981_Silicon-carbon_nanocomposite_pyrolyzed_from_phenolic_resin (accessed Sep. 12, 2020).

[67] E. Bayrakdar, T. Gürkaynak Altınçekiç, and M. A. F. Öksüzömer, ‘Effects of PVP on the preparation of nanosized Al2O3 supported Ni catalysts by polyol method for catalytic partial oxidation of methane’, *Fuel Processing Technology*, vol. 110, pp. 167–175, Jun. 2013.

[68] ‘Solvothermal synthesis of crystalline nickel oxide nanoparticles | Request PDF’, *ResearchGate*. https://www.researchgate.net/publication/229220358_Solvothermal_synthesis_of_crystalline_nickel_oxide_nanoparticles (accessed Aug. 30, 2020).

[69] W. A. W. Abu Bakar, R. Ali, and S. Toemen, ‘Catalytic methanation reaction over supported nickel–ruthenium oxide base for purification of simulated natural gas’, *Scientia Iranica*, vol. 19, no. 3, pp. 525–534, Jun. 2012.

[70] M. C. Bacariza, R. Bértolo, I. Graça, J. M. Lopes, and C. Henriques, ‘The effect of the compensating cation on the catalytic performances of Ni/USY zeolites towards CO2 methanation’, *Journal of CO2 Utilization*, vol. 21, pp. 280–291, Oct. 2017.

[71] B. Coughlan and M. A. Keane, ‘The effects of the environment on the growth of nickel metal particles supported on a range of Y zeolites prepared by ion exchange and impregnation’, *Zeolites*, vol. 11, no. 1, pp. 2–11, Jan. 1991.

[72] K. Stangeland, D. Y. Kalai, H. Li, and Z. Yu, ‘Active and stable Ni based catalysts and processes for biogas upgrading: The effect of temperature and initial methane concentration on CO2 methanation’, *Applied Energy*, vol. 227, pp. 206–212, Oct. 2018.

[73] M. C. Bacariza, I. Graça, J. M. Lopes, and C. Henriques, ‘Enhanced activity of CO2 hydrogenation to CH4 over Ni based zeolites through the optimization of the Si/Al ratio’, *Microporous and Mesoporous Materials*, vol. 267, pp. 9–19, Sep. 2018.

[74] A. Cesaro and V. Belgiorno, ‘Combined Biogas and Bioethanol Production: Opportunities and Challenges for Industrial Application’, *Energies*, vol. 8, no. 8, Art. no. 8, Aug. 2015.

[75] N. Miskolczi, T. Juzsakova, and J. Sója, ‘Preparation and application of metal loaded ZSM-5 and y-zeolite catalysts for thermo-catalytic pyrolysis of real end of life vehicle plastics waste’, Journal of the Energy Institute, vol. 92, no. 1, pp. 118–127, Feb. 2019.

[76] S. Peng, J. Liu, Q. Li, J. Zhang, and Q. Niu, ‘PVP-stabilized Ru colloidal nanoparticles by solvothermal synthesis: Preparation, characterization, and catalytic properties’, Integrated Ferroelectrics, vol. 170, no. 1, pp. 83–91, Mar. 2016.

[77] K. Anandan and V. Rajendran, ‘Morphological and size effects of NiO nanoparticles via solvothermal process and their optical properties’, Materials Science in Semiconductor Processing, vol. 14, no. 1, pp. 43–47, Mar. 2011.

Annex

Appendix 1

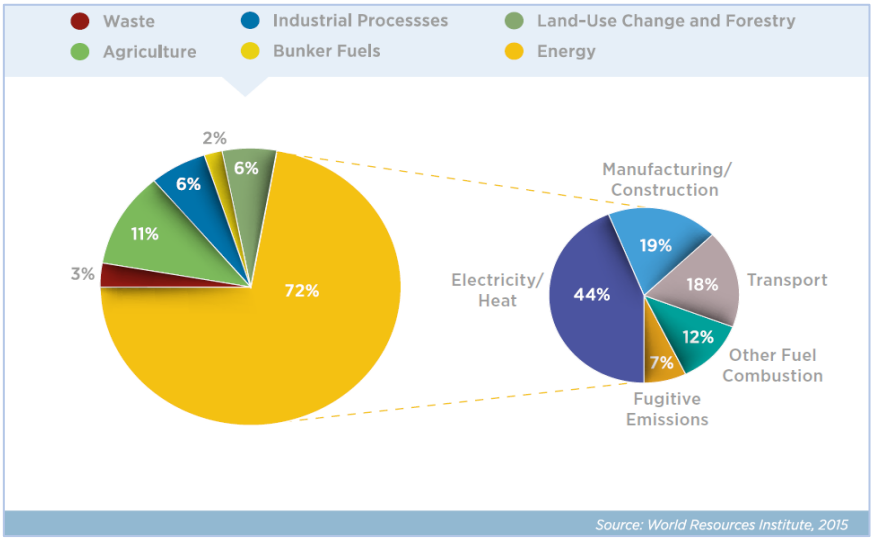

Figure A1: Global Greenhouse Gas Emissions by Sector (2012) [7].

Appendix 2

The composition of different types of biomass in terms of lignocellulosic contents and their methane potential is shown in table A1 below.

Table A1: Composition and Methane Potential of Different Types of Biomass [74].

Biomass	Cellulose [%]	Hemicellulose [%]	Lignin [%]	Methane potential [Nm^3_{CH4}/t_{VS}]
Bagasse	38.2	27.1	20.2	NA
Barley straw	37.5–45	24.2–31.7	9.0–26.1	226.4
Corn stover	33.7–41.3	22.4	15.2–18.6	80–157.3
Eucalyptus	38.0–45.0	12.0–13.0	25.0–37.0	NA
Leaves	11.1–12.2	-	22.7–23.1	47–75
Maize	37.5	30.0	10.3	418
Pine wood	26.0–44.15	30.5	24.3–28.3	20
Rice straw	32.0–39.6	18.5–24.0	13.0–22.7	302
Sorghum	22.2	19.4	21.4	286–319
Sugarcane	25.0	16.8–32.2	12.0–31.4	278
Sunflower stalk	31.0	15.6	29.2	231–297
Switch grass	31.0–45.0	20.0–31.0	12.0–18.0	125
Wheat straw	32.3–37.9	21.2–25.8	8.3–23.4	130–290

Appendix 3

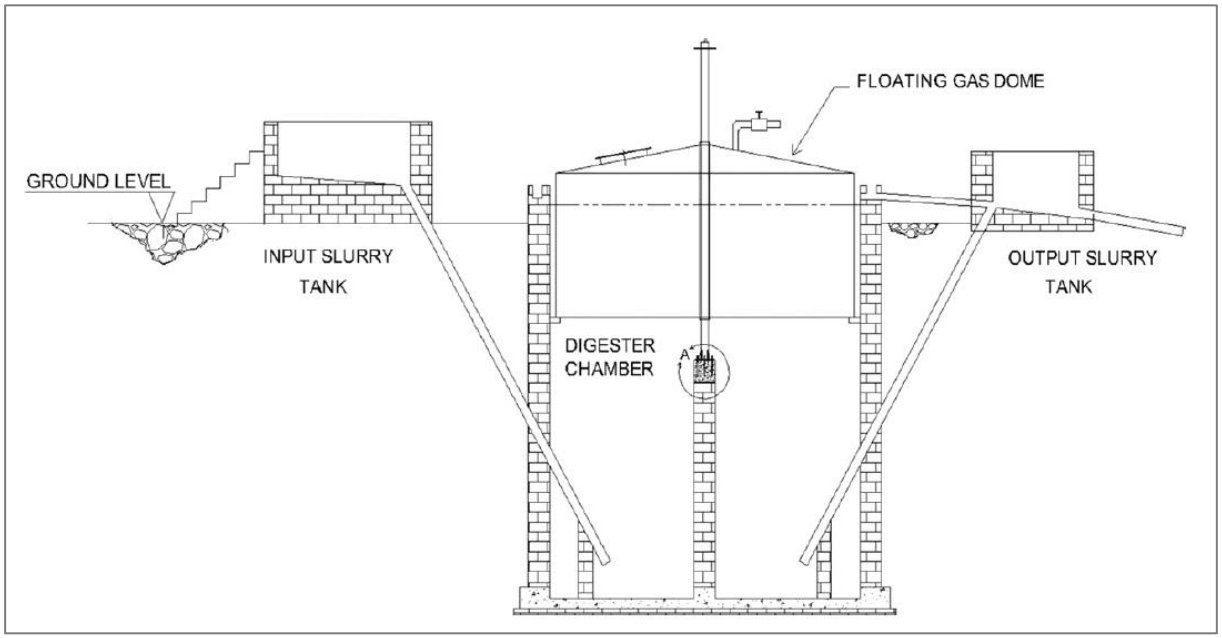

Figure A2: Schematic Diagram of a typical biogas digester [14].

Appendix 4

Physical Scrubbing

Working Principle

- CO_2 is more soluble than CH_4 according to Henry's Law
- Raw biogas flow through a counter flow of a liquid in a column
- Liquid absorb CO_2 leaving biogas with high content of CH_4

Type of Liquid

- Water for water scrubbing
- Polyethylene glycol (PEG)/ Selexol™ and Genesorb™ for organic scrubbing

Current Status

- The most operated biogas upgrading plant among the IEA Bioenergy Task 37 member countries
- As of 2015, 152 units were operated

Feature	Water	PEG
Power demand (€/m³ biogas)	0.25	0.32
Pre-treatment	None	None
Operation pressure (MPa)	0.4-1	0.4-0.8
Outlet Pressure (MPa)	0.7-1	0.13-0.75
Temperature (°C)	40	55-80
CH_4 losses (%)	< 2	2-4
CH_4 purity (%)	96-98	96-98
Post-treatment	Drying	None

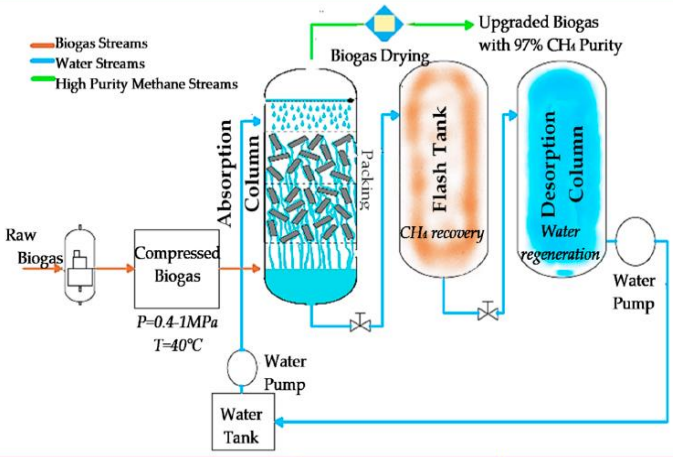

System Upgrading	Advantages	Disadvantages
• Absorption column filled with packing material to increase mass transfer • Flash tank installation to recover trace of CH_4 • Water/PEG regeneration to remove CO_2 for reuse purpose	• Simple process • High methane purity • Less methane loss • Low operation and maintenance cost	• Required huge amount of water • High energy needed • Chances of biological contamination • Required external heat

Figure A3: Physical Scrubbing Technology [31].

Chemical Scrubbing

Working Principle

- CO_2 is more reactive than CH_4
- Raw biogas flow through a counter flow of a chemical solution in a column
- Reaction rate between CO_2 and chemical solution is directly proportional with temperature
- Chemical solution absorbs CO_2 leaving biogas with high content of CH_4

Type of Chemical

- Mono ethanol amine (MEA) or di-methyl ethanol amine (DMEA) for amine scrubbing
- Alkaline solution for inorganic solvent scrubbing
- Different type of solution resulting in different CH_4 purity

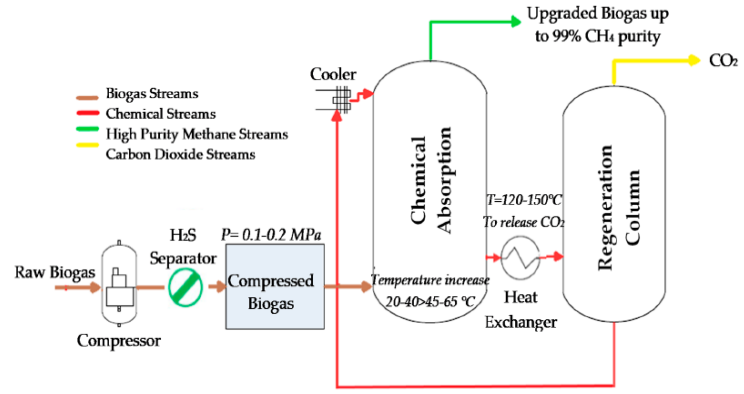

Current Status

- Chemical scrubber was joint second with membrane separation as the most operated biogas upgrading units
- As of 2015, 88 plants were operated

Feature	Description
Power demand (€/m³ biogas)	0.42
Pre-treatment	H_2S
Operation pressure (MPa)	0.1-0.2
Outlet Pressure (MPa)	0.4-0.5
Temperature (°C)	Up to 180
CH_4 losses (%)	<1
CH_4 purity (%)	>99

Advantages

- More CO_2 dissolved per unit volume
- High methane purity
- Low methane loss
- Faster process than physical scrubbing

Disadvantages

- High energy needed to produce steam
- Pre-treatment required
- Difficulties in handling solvent
- Salt precipitation, foaming and poisoning of amine

Figure A4: Chemical Scrubbing Technology [31].

Pressure Swing Adsorption

Working Principle

- CO_2 adsorb on surface of an adsorbent by the van der Waals forces
- Pressure increase result in gas adsorbed and vice versa
- Four steps: adsorption, depressurization, desorption and pressurization

Adsorption Techniques

- Pressure swing adsorption (PSA)
- Temperature swing adsorption (TSA)
- Electrical swing adsorption (ESA)

Adsorbent Material

- PSA: Carbon, zeolites
- TSA: Carbon cryogel microspheres (CCM) and carbon xerogel microspheres (CXM)
- ESA: Activated carbon

System Upgrading

- Multiple adsorption tank installed to ensure a continous operation

Current Status

- Fourth most operated biogas upgrading techniques with 88 units operating (data from 2015)

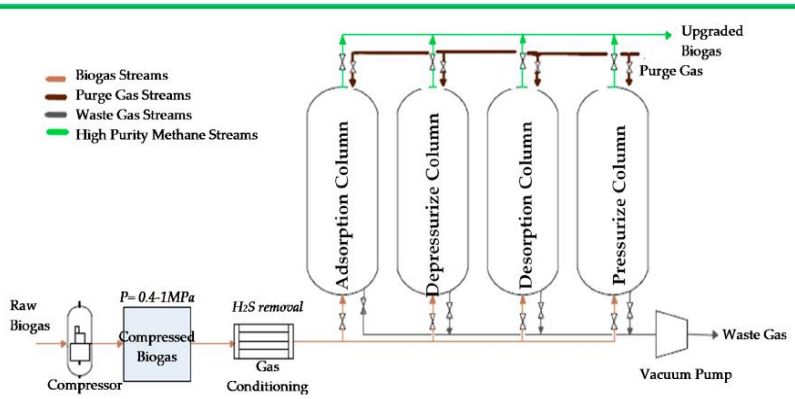

Feature	Description
Power demand (€/m³ biogas)	0.25
Pre-treatment	H_2S
Operation pressure (MPa)	0.4-1
Outlet Pressure (MPa)	0.4-0.5
Temperature (°C)	-
CH_4 losses (%)	<4
CH_4 purity (%)	96-98

Principle of TSA & ESA

- TSA: Temperature is increased at constant pressure to regenerate adsorbent
- ESA: Passing electricity through a conductor to generate heat; alternative for TSA due to higher efficiency in heating and cooling

Advantages

- High gas quality
- Low methane losses
- Dry process
- Low energy demand
- No chemical use

Disadvantages

- Complex process
- Pre-treatment needed
- A couple of streams needed to increase biogas quality

Figure A5: Pressure Swing Adsorption Technology [31].

Membrane Separation

Working Principle

- Separation of biogas components using membrane as permeable material
- The selection of permeability properties of membranes is crucial
- Ascending order of permeation rate: CH_4, N_2, H_2S, CO_2 and H_2O

Separation Techniques

Gas-gas separation (dry)	Gas-liquid separation (wet)
• H_2S and oil vapours were first removed • Biogas is pressurized and injected into membrane	• Liquid and gases separated by membrane • Impurity in the gases absorbed by the counter-current flows of liquid

Type of Membranes

Organic polymers	Non-polymer
• Polyimide (PI) • Cellulose acetate (CA)	• Zeolite • Activated carbon • Silica • Metal-organic framework

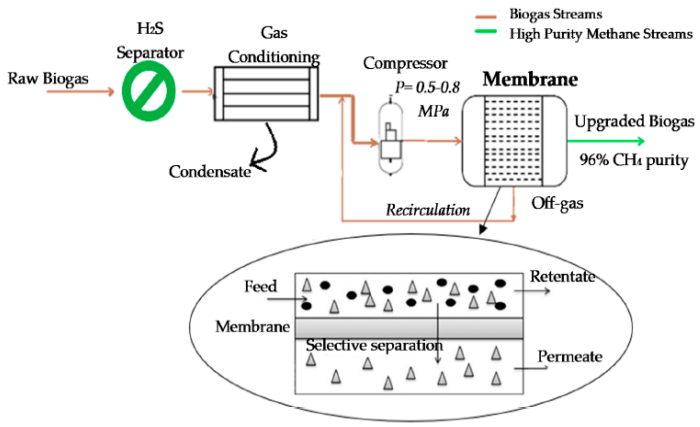

Increasing Efficiency

- Enhanced the CH_4 purity by using two or three-stage performance
- Ideal membrane must have high permeability difference between CO_2 and CH_4

Feature	Power Demand (€/m³ biogas)	Pre-treatment	Pressure (MPa)		CH_4 losses	CH_4 purity
			Operation	Outlet		
Description	0.50	Yes	0.5-0.8	0.4-0.6	<1 %	92-96 %

Advantages	Disadvantages
• Environmental friendly • Low energy consumption • Low cost • Simple process	• Low membrane selectivity • Pre-treatment necessary • Low CH_4 purity

Current Status: Joint second with chemical scrubber for most operated biogas unit as of 2015 with 88 units operating

Figure A6: Membrane Separation Technology [31].

Cryogenic Separation

Working Principle

- Different gases condense at different temperature-pressure domains
- Boiling point of CO_2 was higher than the CH_4 thus allowing the separation
- Biomethane produced by gradual decrease of temperature and compressing the biogas
- Equipment: Compressor, turbine, heat exchanger, and cooler

Boiling Point

Pressure	CO_2 (°C)	CH_4 (°C)
Atmospheric	-78.2	-161.5
1 MPa	-40	-123
Critical pressure:		
CO_2= 7.38 MPa	31.21	n/a
CH_4= 4.60 MPa	n/a	82.44

Post-treatment

- Final product is in accordance with the quality standards for Liquefied Natural Gas (LNG)
- Further cooling for purification will produced Liquid Biomethane (LBM)

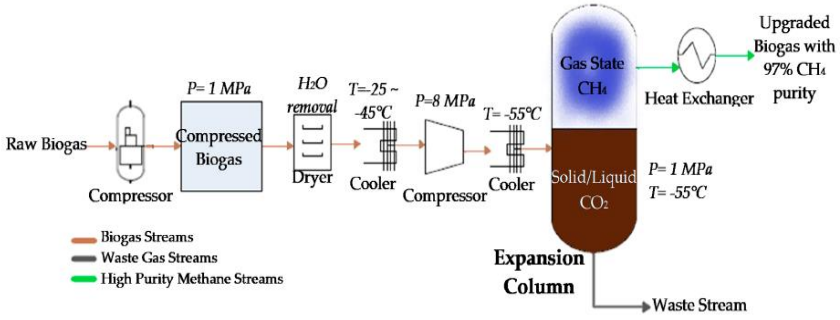

Feature	Description	Advantages	Disadvantages
Power demand	n/a	• High gas quality • Low methane losses • Environmentally friendly • Produce LBM with low extra energy	• High investment and operational cost • Pre-treatment needed • High energy required for cooling • Technology is still under development
Cost	High		
Pre-treatment	H_2O		
Operation pressure (MPa)	1-8		
Outlet pressure (MPa)	0.8-1		
Temperature (°C)	-25~-110		
CH_4 losses (%)	<2		
CH_4 purity (%)	97-98		

Current Status: Only one operating unit making it the most underutilize technique

Figure A7: Cryogenic Separation Technology [31].

Appendix 5

Detailed procedure for determining the catalytic performances

During the catalytic experiences and according to the figure presented below, several data were recorded: temperature ($T_{reaction}$), [CO_2], [CO] and [CH_4] in vol.% and Q_{outlet}.

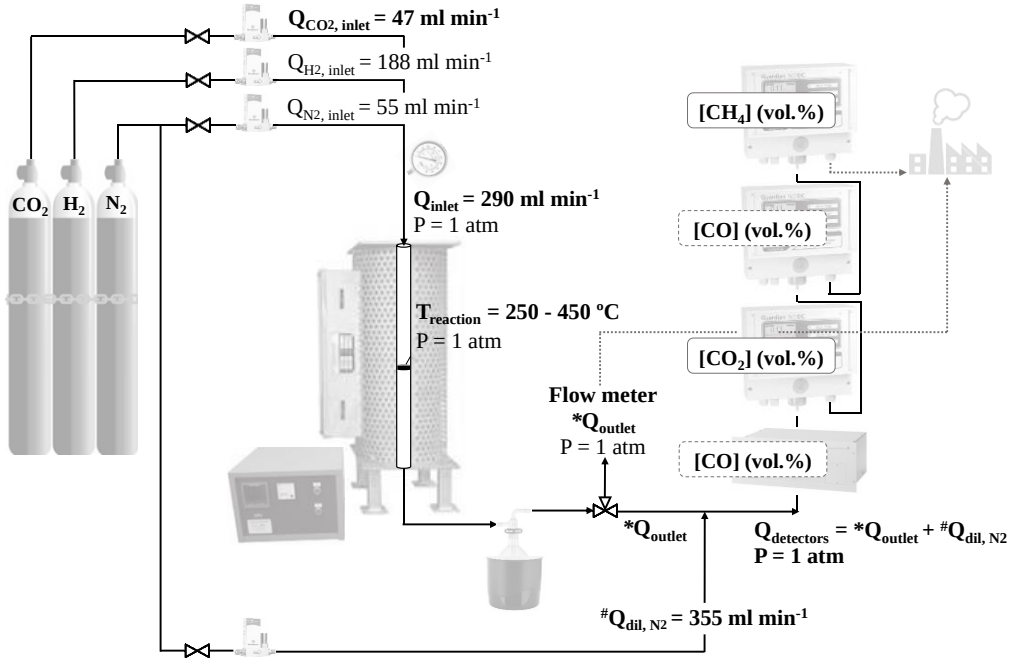

Figure A8: Scheme of the data analysis procedure.

All the flows were measured at the same conditions (T, P) using the flowmeter present in one of the lines coming from the 3-ways valve. Indeed, the inlet volumetric flows of the reactants in absence of reaction (total flow of 290 ml min^{-1} with 188, 47 and 55 ml min^{-1} of H_2, CO_2 and N_2, respectively), were measured passing the gases through the reactor without catalyst, heating at the same reaction temperatures studied in the tests and, finally, passing through the water trap before reaching the flowmeter (Qinlet). Thus, it was guaranteed that the conditions (P, T) used for the measurement of the outlet flows with and without reaction were the same. Additionally, under reaction conditions and with a catalyst in the reactor bed, the outlet flows in dry base (Q_{outlet}) and the reactants concentrations ([CO_2], [CO] and [CH_4]) were measured in the flowmeter and in the detectors, respectively, after passing through the water trap. As a result, and according to the ideal gases equation, it will be equivalent to use volumetric or molar flows for the determination of the catalytic performances. Additionally, the incorporation of a fixed flow of inert ($Q_{dil,N2}$ = 355 ml min^{-1}) in the stream going to the detectors has to

be taken into account. The calculation of the conversion and selectivity for a certain Treaction was done in three steps:

a. Determination of the $Q_{detectors}$:

$$Q_{detectors}\,(ml/min) = Q_{outlet} + Q_{dil,N2} = Q_{outlet} + 355 \qquad \text{Equation A1}$$

b. Conversion of the [CO_2], [CO] and [CH_4] (vol.%) into $Q_{CO2,outlet}$, $Q_{CO,outlet}$, $Q_{CH4,outlet}$ (as the dilution stream contains only N_2, the flow of the reactants in the detectors flow will be the same than in the outlet flow in dry base (after removing water):

$$Q_{CO2,outlet}\,(ml\ min^{-1}) = Q_{CO2,detectors} = [CO_2] \cdot Q_{detectors} \qquad \text{Equation A2}$$

$$Q_{CO,outlet}\,(ml\ min^{-1}) = Q_{CO,detectors} = [CO] \cdot Q_{detectors} \qquad \text{Equation A3}$$

$$Q_{CH4,outlet}\,(ml\ min^{-1}) = Q_{CH4,detectors} = [CH_4] \cdot Q_{detectors} \qquad \text{Equation A4}$$

c. Calculation of the conversion and selectivity with the volumetric flows (as the P, T conditions of the measurements were the same):

d. $$CO_2\ conversion\ (\%) = \frac{Q_{CO_2,inlet} - Q_{CO_2,outlet}}{Q_{CO_2,inlet}} \cdot 100 \qquad \text{Equation A5}$$

e. $$CH_4\ selectivity\ (\%) = \frac{Q_{CH_4,outlet}}{Q_{CO_2,inlet} - Q_{CO_2,outlet}} \cdot 100 \qquad \text{Equation A6}$$

f. $$CO\ selectivity\ (\%) = \frac{Q_{CO,outlet}}{Q_{CO_2,inlet} - Q_{CO_2,outlet}} \cdot 100 \qquad \text{Equation A7}$$